Stitching genomics data to protein structures: Virulence factors in non-O157 Shiga toxin-producing *Escherichia coli*

Sony Malhotra[1], Ashley Ward[2,3,], Lauren Giles[1], Tom Gerrard[4], Martyn Winn[1*], and Nicola Holden[2*]

[1]Scientific Computing Department, Science and Technology Facilities Council, Research Complex at Harwell, Didcot, OX110QX, United Kingdom.
[2]School of Veterinary Medicine and Biosciences, Scotland's Rural College, Aberdeen AB21 9YA, United Kingdom
[3]School of Veterinary Science, University of Liverpool, Department of Livestock and One Health, Neston CH64 7TE, United Kingdom
[4]University of Bristol, School of Cellular and Molecular medicine, Biomedical Sciences building, University Walk, Bristol, BS8 1TD and University of the West of England, School of Applied Sciences, Frenchay Campus, Coldharbour Lane, Bristol, BS16 1QY, United Kingdom

*corresponding authors: martyn.winn@stfc.ac.uk, nicola.holden@sruc.ac.uk

Abstract

The genetic diversity of the Shiga toxin-producing *Escherichia coli* (STEC) sub-species group poses major challenges for assigning pathogenic potential, and for accurate diagnostics. Although existing risk-based frameworks work for the predominant serotypes e.g. STEC O157 or O26, they are less useful for more diverse genotypes, with variation in the genetic complement of virulence factors that is responsible for disease outcome. Moreover, genetic diversity occurs at the virulence factor allele level. We investigated the functional potential of genetic variation at a whole genome level and at an allele variant level, based on the premise that genomic variability underlies phenotypic traits including disease outcomes. We analysed 286 non-O157 STEC genomes for their virulence factor complement and determined co-occurrence patterns. Genetic variation in the well-characterized virulence factor intimin (*eae*) and its receptor (*tir*) was analyzed at a sequence level, and by modelling the three-dimensional protein–protein complex using AlphaFold3 and homology modelling. Different subtypes of Eae were shown to preserve their interaction with the receptor Tir by retaining the interactions at the protein-protein interface. The study shows that virulence factor characterisation in association with 3-D modelling of protein complexes can aid genomic analysis for risk assessment, and inform on functional mechanisms for pathogenicity.

1. Introduction

Shiga toxin-producing *Escherichia coli* (STEC) are a group of foodborne pathogenic bacteria that are predominantly transmitted to humans through contaminated food or from direct contact, particularly from farmed ruminant animals. Diseases caused by STEC range from diarrhoea (D), blood diarrhoea (BD) to more severe haemolytic uremic syndrome (HUS). Animals harbouring STEC do not typically demonstrate signs of infection, creating barriers to risk identification. Transmission of the pathogens through environmental routes, like water, creates a risk of infection from ready-to-eat produce. Treatment of infected patients is limited as antibiotic usage is (for the most part) contra-indicated due to increased risk of release of the Shiga toxin. As such, risk management with surveillance of multiple critical control points is the main means to prevent STEC transmission into the food chain.

Detection of the STEC group of pathogens is challenging due to their serological and genetic diversity. Serotypes other than O157 are increasingly detected and have become more prevalent[1,2], with >338 detected in clinical infections[3]. In many European nations, serogroup O157 continues to be associated with the highest number of HUS cases, hospitalisation and bloody diarrhoea, followed by O26[4]. Identification of pathogenic non-O157 STEC is complicated as not all have the ability to cause disease[5]. As such, there is a pressing need for methods that can first identify them easily, and second, accurately indicate the likely level of risk.

Risk classification of STEC is currently based on the carriage of a particular set of virulence genes, as defined by a Joint FAO / WHO Expert Meeting on Microbiological Risk Assessment (JEMRA) Group[6]. The set of criteria and resulting decision tree (known as the JEMRA STEC risk matrix) are universally used as a means to classify pathogenicity, based on the Shiga toxin (*stx*) variant and carriage of adherence factors including initimin (*eae*) and / or Aggregative Adherence Fimbriae (*aaf*) adhesin (*aggR*). Hazard classification took into account other putative adherence factors, different serotypes and hybrid pathotypes of *E. coli*[6]. The JEMRA risk classification matrix can be supplemented by ranking risks associated with outcomes of clinical disease severity[4] and using them as predictors for disease[7], also based on *stx* variant and carriage of *eae*. The presence of *stx2* is strongly associated with severe disease progression, with highly enhanced potency compared to *stx1*[8]. Subclasses of *stx* can bind different glycosphingolipid receptors, although Gb3 is the principal entry point[9]. The *eae* gene is located on the 35-kb LEE[10] (locus of enterocyte effacement) pathogenicity island along with other effectors and genes for the type 3 secretion system (T3SS). The presence of *eae* together with *stx*2 is commonly used as a molecular signal

to predict pathogenic outcome in clinical settings[11,12]. Intimin (Eae) binds to the translocated intimin receptor (Tir), with the corresponding *tir* gene also located on the LEE. Tir is injected by the T3SS into host cells[13] and embeds itself into the host membrane so that it can bind Eae[14]. For enterohaemorrhagic strains (EHEC *i.e.* most STEC), this is a precursor to the formation of attaching and effacing (A/E) lesions and actin-filament rearrangements resulting in pedestal formation[15]. Similarly in enteropathogenic *E. coli* (EPEC, a different diarrheagenic *E. coli* that is also characterised by A/E lesions but does not encode the Shiga toxin gene), *eae-tir* also facilitates intimate host binding[16].

It is notable that a relatively high proportion of hospitalisation and bloody diarrhoea disease occur in the absence of *eae* carriage[4]. As the minimum virulence gene repertoire is still unclear, computational methods based on genomic content are now being tested to help with this determination. Machine learning approaches have predicted that serious disease (BD and HUS) is associated with additional factors in the O157 serotype beyond established virulence factors[17].

The numbers of STEC serotypes other than O157 is increasing year-on-year across the UK, and in some regions has become more dominant. In England, there were 2,762 total cases of non-O157 STEC reported in 2024, an increase of 22% from 2023 and 175% compared to 2019[1]. In contrast, there were 564 confirmed cases of STEC serotype O157 in England (2024[1]), a decrease of 26% compared to 2022[18]. The same trend is seen in Scotland with increasing non-O157 STEC, of 182 laboratory reports in 2023[2] compared to 170 in 2022[18]. The level of STEC serotype O157 is proportionally lower in Scotland, with 133 laboratory reports in 2023, an decrease from a spike of 270 reported in 2022 (PHS GIZ 2020-2021 report[19]). In European member states there has been a continuous increase in serogroups O26, O146, O145, and O103, although O157 remains the most frequently reported (19%)[20]. The main non-O157 STEC serotypes that are associated with clinical disease include O26:H11 and O145:H28 (as listed in Enterobase[21], 1952-2024, Table S1). Genomic diversity that occurs between serotypes encompasses surface factors affecting attachment phenotypes, virulence factors affecting pathogenicity and host colonisation, and horizontally acquired elements including prophage, insertion elements and plasmids[22].

Genomic variation is a reflection of selection pressure on the gene products and corresponding protein function. This occurs where a genomic complement or gene allele type has been under positive selection in a given environment or host, and so represents the successful clone. In turn, it raises the possibility that such genomic variation can be used to indicate particular traits as a result of host or habitat niche adaptation, such as pathogenicity within a human host or

colonisation of secondary hosts. This broad principle has been applied to another set of pathogens, *Salmonella* species, where machine learning has been applied to protein functional domains to assign biomarkers related to disease severity potential[23].

To investigate the pathogenic potential of less well characterised non-O157 STEC, a set of clinical isolates (n=286) was collated and the key virulence factors identified through genome analysis. A reference panel of known virulence factors[24,25] was used to map these isolates for the presence and distribution of the corresponding genes. Co-occurrence patterns of these genes were then assessed to explore possible functional relationships that may dictate their pathogenic potential. As expected, the *eae* and *tir* virulence genes, associated with A/E lesions, were consistently associated, indicating the presence of the LEE pathogenicity island in a subset of isolates[26]. Within this subset, we could identify multiple eae subtypes and further allelic variation within the subtypes.

We propose that the genomic variability underlying such traits can be used in diagnostics applications. Therefore, investigating allelic variations can help understand their impact on potential protein function and pathogenicity. Three-dimensional protein structure modelling (using AlphaFold3[27]) was used to model the Intimin-Tir complexes and map the allelic variations onto the structures for assessing the impacts on protein structure and function.

2. Materials and Methods

2.1 Data Collection

Human (clinical) isolates were selected from Enterobase[21] (queried Dec 2024), using the following filters:

a. Geographical location: United Kingdom; UK; Great Britain; GB; England; Scotland; Wales; Northern Ireland /NI (but not 'Ireland')
b. Source type: Human
c. '*E. coli'* only and Species: exclude all isolates including "*Shigella*"
d. Serotype filter: anything with O and H type included, all other descriptors removed. Included ones with O type only, removed all blanks or listed as 'Escherichia coli'. All the O157 were removed as the focus of this study is non-O157.
e. Path/Non path: Pathogenic & blanks included
f. Pathotypes related to UTI or ExPEC removed. Included EIEC.
g. Lab contact: Anything that contain 'Public Health England' included in email addresses
h. Collection year: from 2010 onwards

These entries in Enterobase do not have clinical outcome data because questionnaires are not routinely administered to non-O157 cases in the same way as they are STEC O157 cases (pers. communication Claire Jenkins).

Within the non-O157 STEC dataset, O26 STEC isolates were eliminated as it is the most prevalent non-O157 STEC serotype in the UK[1,2] and could disproportionately skew the dataset and subsequent analyses. Furthermore, O26 is already one of the most extensively characterized non-O157 serotypes. The aim was to obtain a broader snapshot of recently emerged and less-characterized strains. After applying the filters described above and removing O26, to further capture H-antigen diversity and maximise the diversity of serotypes, an isolate per H-antigen type was selected for each non-O157 serotype.

Further, these isolates were filtered for the presence of *stx* gene to identify the (non-O157) STEC genomes. For this, the paired end reads from Sequence Read Archive[28] (SRA) were downloaded

using the fastq-dump utility, and filtered using the BBTools[29]. The following criteria were used for cleaning the downloaded reads:

i. discard reads with average quality below 20.
ii. Trim adapters based on pair overlap detection (does not require known adapter) using BBMerge
iii. Trim both reads to the same length
iv. Also used the generalized adapters and trimmed provided by BBTools package which includes Illumina Truseq and Nextera adapter sequences

The obtained cleaned reads were then mapped to the *E. coli* stx gene sequences downloaded from the VirulenceFinder 2.0 (as described in section 2.2), using bowtie2[30] and samtools[31]. The downloaded set of stx sequences from VirulenceFinder 2.0 cover a variety of stx subtypes and include subtypes stx1a, stx1c, stx1d, stx1e, stx2a, stx2b, stx2c, stx2d, stx2e, stx2f, stx2g, stx2h, stx2i, stx2j, stx2k, stx2l, stx2m, stx2n and stx2o.

The resulting stx+ genomes were assembled using the Shovill pipeline (https://github.com/tseemann/shovill) and the Spades assembler[32] which scans over multiple kmer lengths. Prokka[33] was used to annotate the assembled genomes and identify genes.

2.2 Virulence Factors Mapping

The list of *E. coli* virulence factors (virulence_ecoli.fsa) was downloaded from the Virulence Finder 2.0[24,25] (database version 2022, last updated in April 2024, https://bitbucket.org/genomicepidemiology/virulencefinder_db/src/master/). For some of the virulence factors such as intimin (*eae*), the downloaded annotations include the subtype mapping. The whole list comprises 4942 sequences of virulence factors including the subtypes and their multiple sequences, which maps to 680 sequences for different subtypes of virulence factors by removing alleles.

Virulence Finder provides a very broad list that includes any factor associated with pathogenicity, but many are simply colonisation factors and not true virulence genes. The sequence identity between related entries can also be high. Thus, *stx1* and *stx2* subtypes are just a few SNPs different and there can be multiple subtypes per genome which may cause the assembly to split the gene.

An in-house database was built using BLAST[34] for the reference virulence factor sequences which was then used to search for virulence factors in the Prokka-annotated isolate genomes. tblastn[35] was used to query the database with an evalue cut off 10^{-4}. The hits were then filtered using the following criteria:

1. percent identity >=90%
2. query coverage >= 75%, where query coverage is the aligned query/length of query

Using these two filters if a sequence maps to more than one virulence factor gene, the hit with the greatest percent identity was selected. Further filtering was done using the subject (virulence factor gene) coverage cut off of >=75%, where subject coverage is the aligned subject/subject length to filter out the genome sequences which are just partial sequences.

For isolates carrying the intimin gene, the main genetic subtype (alpha, beta, gamma, etc) was identified based on the Virulence Finder annotation of the closest sequence match, noting that the database includes several entries for each subtype. Although Virulence Finder contains sequences for the intimin receptor, encoded by the *tir* gene, there is no equivalent subtype annotation for these entries.

The term ‘variant’ is used throughout the text and is defined in context, with respect to STEC serotype, gene presence/absence at the genome level, specific gene subtypes, or within gene point mutations.

2.3 Co-occurrence of virulence factors

Entries in a co-occurrence matrix were defined as the number of isolates in which a pair of virulence factors occur together, normalised by the total occurrence of the virulence factor on the row, so that the matrix is asymmetric with respect to the two virulence factors. An enrichment factor was also defined of a virulence factor *A* with respect to a virulence factor *B* as the ratio of the occurrence of *A* in *B*+ isolates to its occurrence in *B*- isolates, adjusted for the relative number of each group of isolates:

Enrichment of virA in presence of virB: $E_A^{(B)} = (virAB/virB) / ((virA – virAB) / (286 – virB))$

198 A value greater than one implies that a virulence factor *A* is more likely to be found in an isolate
199 containing *B* than one where *B* is absent. The Jaccard similarity was also considered, J_{AB}, defined
200 as the number of isolates containing both virulence factors divided by the number of isolates that
201 contain at least one.

202 2.4 Sequence alignment and phylogenetic trees

203 Sequence alignments were performed using MUSCLE[36]. RaxML[37] was used to generate
204 phylogenetic trees for different sets of sequences. For extracting the LEE island, the LEE
205 sequence from the *E. coli* O157:H7 strain Sakai (GenBank accession no. BA000007) was used.
206 BLAST[34] against the Sakai sequence was performed using all the contigs from the *eae*+
207 genomes. A contig was considered to contain a LEE island if it shared at least 80% sequence
208 identity with the Sakai LEE sequence and the alignment length was at least 20 kb. The LEE
209 sequences were extracted from the *eae*+ isolates (n=85) and the pangenome was built using
210 Panaroo[38].
211
212 The pangenome for the *stx*+ isolates (n=286) was built using Panaroo[38] and the annotation
213 previously output from Prokka. RaxML (v8.2.12)[37] was used to build an alignment of the core
214 genome. Visualisation of the annotated trees was done in Iroki[39].
215
216 Sequence alignments were used as an input to SplitsTree[40] to compute a split decomposition
217 network (selecting network -> split decomposition).

218 2.5 Three dimensional structural modelling of virulence factors

219 AlphaFold3[27] was used to model the structures of protein complexes. The protein sequences of
220 Eae (D1, D2 and D3 domains) and Tir (Tir intimin binding domain) in Fasta format were used as
221 input to the AlphaFold3 server (https://alphafoldserver.com/). In total, ten subtypes of Eae were
222 modelled using sequences taken from isolates for which the subtype had been identified, with the
223 cognate Tir sequence taken from the same isolate. The following accession IDs were used for
224 structural modelling of Eae subtypes: alpha:SRR3581427, beta:SRR4180889,
225 gamma:SRR3581353, rho:SRR3241980, theta:SRR4179996, epsilon:SRR3574270,
226 xi:SRR16203499, delta:SRR29176816, iota:SRR4195732 and zeta:SRR4184837. For each
227 subtype, a separate job was run, using the Eae protein sequence as entity 1 (copy = 1) and the
228 Tir protein sequence from the same genome as entity 2 (copy = 1). The server returns top five

229 scoring complexes and the one with highest ranking_score was selected. Ranking_score
230 combines pTM (predicted TM-score for full structure), ipTM (predicted interface TM-score),
231 penalises clashes and encourages the absence of spurious helices in disordered regions[27].
232
233 Additional homology based structural models were built for some of the subtypes (rho and theta)
234 using Modeller (v9.10)[41]. The template used for the homology modelling is PDB ID: 1F02 and the
235 model with lowest DOPE (Discrete Optimised Potential Energy) score was selected as the best
236 model.
237

3. Results

3.1 Collation of STEC isolate genomes

3.1.1 Initial download

A retrieval of all E. coli isolates from EnteroBase yielded 86,609 accessions. The filtering criteria described in Section 2.1 (Methods) were applied to retain clinical, non-O157 isolates, resulting in 7,855 isolates. The most common serotypes (Figure 1A) in this subset were O26 (n = 1,027), O145 (n = 554), and O146 (n = 515). The O26 serotype was subsequently excluded because it is already well characterised and overrepresented in public databases. To ensure a broader snapshot of recently emerged and less-characterized strains, one isolate per H-antigen was retained for each remaining non-O157 serotype. This resulted in a filtered subset of 1177 isolates.

Entries in Enterobase do not have clear metadata on pathogenicity or clinical outcome. We make the assumption that all of the human isolate sequences selected from Enterobase using this protocol were associated with clinical disease symptoms, since the isolates in this collection were all deposited by reference or diagnostic laboratories. They are hereafter referred to as ‘clinical isolates’.

3.1.2 Presence of Shiga toxin gene

Isolate genomes could not be filtered in Enterobase by the presence of *stx* gene(s) because of incomplete metadata, nor were they generally designated explicitly as STEC. Therefore, the genome sequence reads were downloaded and mapped to the *E. coli stx* gene alleles from the Virulence Finder v2.0 database[24,25]. Out of the 1177 genomes in the original Enterobase set, 326 genomes had at least one read mapped to one of the *stx* gene subtypes. This does not necessarily imply that all these 326 genomes are true STEC due to the low threshold of number of reads mapped to the *stx* genes. Therefore, confirmation of *stx* presence was carried out at the annotation level following assembly of the 326 genomes.

3.1.3 Filtering for STEC genomes

The 326 putative STEC genomes were assembled and annotated, as described in section 2.1. A more stringent check for the presence of *stx* genes was based on *tblastn* searches, using the protein sequences obtained after the annotation step (section 2.2). As the reference *stx* genes (from Virulence Finder v2.0) includes both subunit A and subunit B genes, the BLAST hits were

267 further validated, and only genomes that included both *stx* toxin A and B subunits were selected.
268 This resulted in 286 *stx*+ isolates, henceforth referred to as non-O157 STEC isolates. The
269 Enterobase accession numbers for these 286 isolates are provided in Table S2. The distribution
270 of *stx* types among serotypes present in more than five isolates is shown in Figure 1B. Sole
271 carriage of *stx2* only occurred in serotype O8 and O80, while conversely sole carriage of *stx1*
272 occurred in O78 and O79 serotypes. All other serotypes (9) encoded both *stx1* and *stx2* subtype
273 reads.

274 3.2 Virulence factor genes in STEC genomes

275 3.2.1 Virulence factors

276 The complete set of virulence factor alleles was mapped onto non-O157 STEC genomes (n=286)
277 using tblastn[35] following the annotation of the assembled genomes (see Section 2.2). For ease of
278 presentation, virulence factors are referred to by their 3-letter gene name, of which there were 85
279 present in the set of non-O157 STEC isolates (Table S3) . Where appropriate, individual genes
280 were identified, of which there were 130 in the genome set when allelic variants were merged
281 (Table S4). Isolate genomes varied in the number of virulence factors identified, and Figure 1C
282 shows the distribution of virulence factor load. The genome with maximum number of virulence
283 factors is accession SRR3579389 with 52 factors mapped to it, in contrast to minimum number of
284 virulence factors (n=12) in the genome of accession SRR29241024.
285
286 For the two main *stx* groups, 128 genomes encoded only the *stx1* subtype, 110 had only *stx2*
287 subtype, and the remaining 48 genomes contained representatives of both *stx1* and *stx2*. Further
288 division into *stx* subtypes was carried out using the reference sequences in Virulence Finder v2.0
289 (Figure 1D). We observed two subtypes of *stx1* (1a and 1c, roughly in equal numbers) and seven
290 subtypes of *stx2* (2a,2b,2c,2d,2f,2g,2k) across the 286 isolates (Figure 1D). Of these seven stx2
291 subtypes, the most common were *stx2b* and *stx2c*, with low numbers of five other subtypes.
292
293 The most frequent virulence factors were assessed, classed as present in at least 50% of the
294 genomes (Figure 2A). *nlpI* (lipoprotein NlpI precursor) and *terC* (tellurium ion resistance protein)
295 are present in all 286 genomes, followed by *yeh* (4 genes, YHD fimbrial cluster) and *csgA* (curli
296 major subunit) which are present in 283 and 281 isolates respectively. Nine other virulence factors
297 are widespread in our set of isolates, though still absent from a significant fraction.
298

299 Co-occurrence of virulence factors was determined for the set of 286 non-O157 STEC genomes
300 (Figure 2B). The co-occurrence values were normalised for a pair of virulence factors by the total
301 occurrence of the virulence factor on the row, so that the matrix is asymmetric with respect to the
302 two virulence factors.
303
304 First, co-occurrence of virulence factors with intimin was a point of focus, as it is one of the key
305 virulence factors for the STEC group[41] in terms of incidence and disease outcome (see row 'eae'
306 in Figure 2B) [42]. To help identify significant correlations with intimin, an enrichment factor $E_A^{(eae)}$
307 was defined as the ratio of the occurrence of a virulence factor in *eae*+ isolates to its occurrence
308 in *eae*- isolates, adjusted for the relative number of each group of isolates. The Jaccard similarity,
309 $J_{A,eae}$, between the set of isolates containing a specified virulence factor and the set carrying *eae*
310 was also considered. Values for all virulence factors are listed in Tables S3 and S4. By these
311 definitions (see Methods), *tir* has $E_{tir}^{(eae)}$ of infinity as it never occurs without its binding partner,
312 and $J_{tir,eae}$ = 1 since it has an identical distribution across the isolates. On the other hand, *etp* has
313 $E_{etp}^{(eae)}$ of infinity as it only occurs in *eae*+ isolates, but $J_{etp,eae}$ = 0.27 since it only occurs in 23 of
314 the *eae*+ isolates and thus has a different distribution.
315
316 The gene group *nleA, nleB, nleC* comprises non-LEE effectors which are functionally dependent
317 on the LEE-encoded T3SS. At least one *nle* gene is found in 83 out of 85 *eae*+ isolates, while all
318 three are found in a single *eae*- isolate. The presence of *eae* and *nle* genes is reported to be a
319 signature for highly virulent STEC strains and are reported to co-occur in non-O157 serotypes[43].
320 *nle* is reported to correlate with outbreak and HUS potential[44].
321
322 For the *cif* gene, 37 out of 38 occurrences are in *eae*+ isolates, while for both *espJ* and *efa1* it is
323 44 out of 45. Several of these genes have been observed on a lambdoid prophage ΦE22[45] and
324 so may be carried together. A single isolate (AIPCOOIH) carries the only occurrences of *nleA,*
325 *nleB, nleC, cif, espJ* and *efa1* that are not associated with intimin.
326
327 Other genes enriched in *eae*+ isolates include *espP*, *tox*, *katP* and the bacteriocin *cia*. Table 1
328 lists other virulence factors that were observed to co-occur with eae, though some are also widely
329 seen in *eae*- isolates. Some of these are toxins (such as hemolysin, enterohemolysin), adherence
330 and colonisation factors (*efa, fdeC*), or help in evading the bacterial complement system (*iss*).
331

332 **Table 1**: Virulence factor genes that show significant co-occurrence with *eae* in non-O157
333 STEC isolates. The co-occurrence is defined as the number of isolates carrying both the
334 virulence factor of interest and *eae*, as a fraction of the total number of *eae*+ isolates,
335 corresponding to the values on the *eae* row of Figure 2B. The following column gives the
336 absolute number of isolates carrying the virulence factor, divided between *eae*+ and *eae*-
337 isolates.
338

Gene co-occurring with *eae*	Co-occurrence	Number in *eae*+ / *eae*- isolates	Short description
cif	0.44	37 / 1	Type III secreted effector
efa1	0.52	44 / 1	EC factor for adherence; lymphostatin *Efa1-LifA*
ehxA	0.76	65 / 105	Enterohaemolysin:known to be associated with HUS and diarrheal disease
espA, espB, espC, espF, espI, espJ, espP, espY	1.00	85 / 48	E.coli secreted protein; *espA*, *espB*, *espF* carried on LEE island; *espP* serine protease
fdeC	0.73	62 / 175	intimin-like adhesin *fdeC*: biofilm formation; structural similarity to intimin
hlyA, hlyE, hlyF	0.67	57 / 98	Hemolysin; known to be associated with HUS and diarrheal disease
iha	0.46	39 / 121	*irgA* homologue adhesin (*Iha*)
iss	0.69	59 / 141	Increased serum survival; complement resistance
lpfA	0.45	38 / 148	Long polar fimbriae: adhesive factor;also known to be expressed in LEE-negative clinical isolates
nleA, nleB, nleC	0.98	83 / 1	Non-LEE effectors
ompT	0.94	80 / 137	Outer membrane protease (protein protease 7):
traJ, traT	0.68	58 / 166	*traJ* (Positive regulator of conjugal transfer operon)) and *traT* (Outer membrane protein complement resistance:);
yghJ	0.73	62 / 132	Secreted and surface associated lipoprotein; aids in colonisation

339
340 In contrast, many pairs of virulence factors are mutually exclusive, meaning that there are no
341 isolates that contain both. This may simply be because of low overall occurrence in the dataset,
342 or may reflect some aspect of genomic structure *e.g.* competition for the same phage integration
343 site. In particular, the genes *subA*, *kpsM*, *pic* and *senB* occur 79, 92, 24 and 67 times respectively,
344 but never in *eae+* isolates. The *subA* gene encodes a component of the SubAB toxin, which has
345 been observed in LEE-negative STEC strains including clinical human isolates[46]. The gene *pic*
346 encodes for a member of the serine protease auto-transporter (SPATE) family and has been
347 shown to have mucolytic activity[47].
348
349 The *ireA* gene occurs in 99 eae- isolates and a single *eae+* isolate (SRR3579389). Similarly, *aal*
350 genes occur in 28 *eae-* isolates and *fae* genes occur in 29 *eae-* isolates, while a single *eae+*
351 isolate (SRR3573434) contains a copy of *aalF, aalH, faeE, faeF, faeC, faeI, faeD*.
352
353 Next, co-occurrence of groups of genes independent of intimin was determined. A co-occurrence
354 matrix for a set of 32 genes was generated (Figure S1). Genes that occur either too rarely or
355 which are very common were excluded, as were those that showed no significant co-occurrence.
356 Several sets of genes were identified that showed a degree of co-occurrence between each other
357 (Figure S1). The largest group consisted of *'ireA', 'kpsM', 'mchC', 'mchF', 'senB', 'shiA', 'sitA',*
358 *'subA', 'tia'*. These are all enriched in *eae-* isolates, and include three of the genes (*subA*, *kpsM*
359 and *senB*) that are never found in *eae+* isolates. Similarly, adhesion-associated locus genes (*aal*)
360 and fimbrial genes (*fae*) are found to co-occur, and are found more frequently in *eae-* isolates.
361
362 Another significant group consists of genes *cif*, *efa1*, *iucC*, *iutA*, *katP*. Three of these were
363 observed above to co-occur with intimin, and therefore will co-occur with each other. Finally, there
364 are pairs of genes which occur together, e.g. the Colicins B and M (*cba*, *cma*), as has been seen
365 previously[47], which are almost always found adjacently on the same large conjugative plasmid.
366 The genes *cba* and *cma* have intimin enrichment factors of 0.26 and 0.43 suggesting a slight
367 enrichment in *eae-* isolates.

368 ### 3.2.2 Intimin (*eae*) subtype mapping

369 Within the set of 85 (30%) isolates that are both *eae* and *stx* positive, several *eae* genetic subtypes
370 can be distinguished (based on their best match upon BLAST searches against the reference *eae*
371 sequences, section 2.2). The *E. coli* virulence factors in the virulence finder database (Section

372 2.2) include 20 subtypes of *eae*: alpha, beta, delta, epsilon, eta, gamma, iota, kappa, lambda, mu,
373 nu, omicron, pi, rho, sigma, tau, theta, upsilon, xi and zeta. Of these, 10 *eae* subtypes were
374 identified in the set of non-O157 *stx*+ isolates; namely alpha, beta, delta, epsilon, gamma, iota,
375 rho, theta, xi and zeta.

376 The *eae*+ genomes were mapped to the *stx* gene subtypes in order to investigate if any *eae*
377 subtype occurrence correlates with *stx* gene type (Figure 3A). 6/85 eae+ isolates possess both
378 *stx1* and *stx2*, while 44 and 35 possess only *stx2* or *stx1*, respectively. Four *stx* gene subtypes,
379 namely *stx1a, stx2c, stx2d* and *stx2f*, co-exist with the *eae* gene. *stx2* has been shown to be
380 associated with severe disease phenotype[49,50] and it is interesting to note that in the non-O157
381 STEC dataset, *eae*-gamma and *eae*-iota co-occur exclusively with the *stx2c* subtype. stx2c is
382 associated with six further *eae* subtypes, although in those cases not exclusively. *stx2d* which is
383 reported to be very virulent in mice and associated with HUS[51] was seen co-occurring mainly with
384 subtype *eae*-xi, but also with *eae*-epsilon. The less virulent form *stx1a* was present with 6 *eae*
385 subtypes.

386 The *stx* subtype mapping for *eae-* isolates (n=201) shows that 21% (n=42) of the isolates possess
387 both *stx1* and *stx2*, while 33% (n=93) and 46% (n=66) of the isolates possess only *stx1* or *stx2*
388 respectively. Further, mapping these to *stx1* and *stx2* subtypes, it is interesting to note that some
389 subtypes (*stx1c, stx2a, stx2b, stx2e, stx2g, stx2k and stx2l*) were exclusively seen in the *eae-* set
390 (Figure 3B).

391 ### 3.2.3 Evolution of the *eae* (intimin) gene

392 Across the set of 85 *stx*+/*eae*+ isolates, there are 31 unique translated intimin sequences,
393 categorised into 10 subtypes. The diversity across the observed intimin sequences is displayed
394 as a heatmap (Figure S2) generated using percent identity values between the protein
395 sequences. The minimum percent identity is between the single iota sequence and two zeta
396 subtype sequences (79.1%) whereas epsilon and xi sequences are most similar with ~97%
397 identity (Figure S2). To understand the evolution of the *eae* gene and the variation within the
398 different subtypes, the intimin subtypes were mapped onto phylogenetic trees. As intimin is
399 encoded by a gene on the LEE island, originally acquired through horizontal gene transfer, we
400 sought to separate different evolutionary drivers by constructing phylogenies at the level of the
401 core genome of *stx*+ isolates (n=286), the whole LEE island of *stx*+/*eae*+ isolates (n=85) and the
402 individual translated intimin sequences (n=31).
403

404 The selected set of non-O157 STEC isolates (n=286) were observed to have a core genome
405 (99% <= strains <= 100%) of only 3119 genes out of the total ~36k genes, with most genes in the
406 shell and cloud regions. This agrees with the known observation of pathogenic *E. coli* genomes
407 to be larger and more diverse than their commensal counterparts[52]. Virulence factors such as
408 *eae*/*tir* are assigned to the cloud region, in accordance with the low level of occurrence
409 (highlighted above). A phylogeny was obtained using the core genome of the isolates, and
410 annotated with the *stx* and *eae* subtypes (Figure 4A). The distribution of *eae* across different
411 clades is consistent with multiple acquisitions of the LEE island via horizontal gene transfer. The
412 phylogeny shows reasonable clustering of the *eae* subtypes, although several subtypes are split
413 across different branches which may be due to inaccuracies in the phylogeny or from
414 recombination events.
415
416 The phylogeny obtained using the full-length LEE sequences from 85 *stx*+/*eae*+ isolates (Figure
417 4B) results in better clustering of the *eae* subtypes compared to the core genome phylogeny,
418 confirming the fundamental role of genomic location. Further, it is interesting to note that the *eae*
419 subtypes cluster even better in a phylogeny derived using only the LEE-located gene for the Type
420 3 secretion system Secretin (Figure 4C). This gene is essential to the function of T3SS, and its
421 evolution is a good measure of that of the LEE island. Identifying the core genome of the LEE
422 island using pangenome analysis (as previously applied to the whole bacterial genome), and
423 constructing a phylogeny based on the set of core genes, produces similar results (Figure S3A).
424 These phylogenies show that evolution of intimin subtypes largely follows evolution of the LEE
425 island, except for some splitting of the beta and theta clades. Finally, a phylogeny was constructed
426 from the 31 unique translated intimin sequences, reflecting only nonsynonymous variations
427 (Figure 4D). This shows perfect separation of intimin subtypes, except for the inclusion of the
428 single delta intimin sequence within the beta clade.
429
430 Next, the evolutionary mechanism of the intimin gene was investigated. While point mutations
431 produce branches in a tree-like pattern, recombination events lead to networks with closed loops.
432 Networks were generated using split decomposition analyses of the full length (Figure S3B), N
433 terminus (1-700 amino acids, Figure S3C) and C-terminus (701-939 amino acids including the D2
434 and D3 domains, Figure S3D) of the intimin sequences, using SplitsTree[40]. These network
435 patterns indicate horizontal gene transfer through recombination is more prominent in the N-
436 terminus of the intimin sequence. Split decomposition analysis using an alternative division into
437 N-terminus (1-550) and C-terminus (551-939 including domains D0, D1, D2 and D3) regions

438 showed a similar trend, with the network using the N-terminus region more reticulate than the C-
439 terminus region (Figure S4).

440 3.3 Structural analysis of exemplar virulence factors: Intimin-Tir

441 3.3.1 Variations in Intimin

442 Allelic variation in *eae* was shown to be associated with STEC genotype, indicating a degree of
443 clonality[53]. While there are no experimental structures of the full-length Intimin and Tir proteins,
444 there are crystal or NMR structures of individual domains. Intimin is usually ~939 amino acids
445 long and comprises a flexible periplasmic N-terminal region (up to ~188 amino acids), followed
446 by the transmembrane beta-barrel domain (189-549) and the extracellular C-terminal region (550-
447 939) (Figure 5A). The super-domain D2/D3 in the C-terminal region is responsible for binding the
448 cognate receptor Tir and forming host attachment. We use residue numbering based on the
449 UniProt reference sequences P19809 (Eae) and Q9KWH9 (Tir), which are represented by the
450 structure PDB ID: 1F02[54]. This reference protein sequence for Intimin has 99.79% identity with
451 the translated sequence of an alpha subtype *eae* annotated in Virulence Finder, although other
452 reference alpha subtypes from Virulence Finder have lower identities down to 86% (illustrating
453 variation within subtypes). The P19809 sequence also clusters with alpha subtype sequences
454 within our set of isolates.
455
456 The 85 intimin protein sequences from our *stx+/eae+* isolates (comprising 31 unique sequences)
457 were aligned to the UniProt sequence P19809 (subtype alpha), resulting in the identification of
458 706 point variations. These were mapped onto the domains using the following domain
459 boundaries: 1-39, 65-115, 189-430, 450-550, 559-653, 658-751, 755-842, 843-939,
460 corresponding to the SP (Signal Peptide), LysM, barrel, D00, D0, D1, D2 and D3 domains
461 respectively (Figure 5A). Overall 661/706 variations lie within these domains, with the rest present
462 in linker regions, and the majority of these (78%) lie in the exposed domains D1, D2 and D3
463 (Figure 5B).
464
465 Residues that contribute to the interface with Tir are different in our isolates to those observed in
466 the P19809 reference sequence (PDB ID: 1F02), with a limited number of variant types permitted
467 (Figure 5C, Table 2). Residue 926 is mutated to a valine in all 85 *eae+* isolates, including those
468 identified as alpha subtype, suggesting a global shift rather than variability. On the other hand,
469 the neighbouring residue 927 shows 8 residue types (including the reference Lys) suggesting

470 more variability at this site. Some of these variants involve a change in the amino acid type and
471 side chain length such as (I897T, I897S, T895I), whereas others involve more subtle
472 physicochemical changes such as I926V, K919R, Y934F, R850K. The variations at the interface
473 are investigated in more detail below (section 3.3.4).
474
475 **Table 2**: Amino acid variations observed in the interface residues in Eae sequences from the
476 dataset of *stx*+/*eae*+ isolates. Residues are ordered according to their observed variability,
477 namely the number of distinct variations with respect to the reference sequence P19809.
478
479

Reference residue (1F02)	Types of variation	Number of isolates with ref residue mutated	Mutated residue(s)
K908	7	85	S, R, T, Q, N, I, P
K927	7	82	G, D, H, T, E, S, N
N924	6	82	P,T, I,A, Q, -
E930	6	85	K, A, T, N, D, S
Q894	5	74	K, L, R, E, N
Q905	5	72	D,A,V, K, S
S909	4	42	Q, G, E, K
N925	4	49	G, S, D, R
L923	4	38	V, R, H, I
I897	3	72	T, S, N
K919	3	70	T, R, A
T895	3	55	S, A, I
R850	3	50	K, Q, P
S929	3	85	K, N, T
I896	2	31	L, M
I926	1	85	V
Y934	1	44	F
V911	1	26	W
A933	1	23	V
D916	1	12	N

480

481

482 ### 3.3.2 Variations in Tir (translocated intimin receptor) protein sequence

483 The cognate receptor of intimin, Tir, is known to be rich in disordered regions, with flexible
484 intracellular domains (*i.e.* N-tir and C-tir) that allow it to engage with a variety of host proteins[55].
485 Tir binds Intimin via its extracellular domain (residues 271-336, using the sequence numbering of
486 PDB ID: 1F02) with much of the interaction mediated by a beta-hairpin (residues 296-315)[56].
487
488 The extracellular domain of Tir was observed to be more conserved than the Tir binding region of
489 Eae. There were 49 variant types of which 15 types are in the beta hairpin of Tir located at 9
490 distinct sites (Figure 5D). All of these variations in beta hairpin were present in less than 50% of
491 the genomes except for the A303E which was observed in nearly all (84) of the eae+ sequences
492 (Figure 5D).
493

494 ### 3.3.3. Structural mapping of Eae variations

495 706 variant types identified in our set of eae+ isolates (section 3.3.1), map to 320 residues.
496 AlphaFold3 was used to model the full length structure of Eae (UniProt ID:P19809, PDBID: 1F02)
497 and these 320 residues (in black sticks) were mapped onto the modelled structure (Figure S5A).
498 The N-terminal region is modeled with low confidence as indicated by poor pLDDT scores (<50
499 or between 50-70). Additionally, higher PAE (predicted aligned error) scores (Figure S5B)
500 suggests that AlphaFold3 is uncertain about the relative positioning of the domains (except for
501 D1,D2 and D3 domains) in the modeled structure. The mapping of observed mutations suggests
502 most of the variations are in the extracellular regions of Eae. This poor quality, low confidence
503 structure is only used to map the sequence variations onto the structure and this low quality
504 structure is not used for drawing any functional or structural implication of these variations.
505
506 The reference crystal structure (PDB ID:1F02) corresponds to domains D1, D2 and D3 (residues
507 658-939) of Eae along with the Eae binding region of Tir (residues 271-336), and we mapped the
508 point variations observed in these regions onto this structure. Figure 5E shows the crystal
509 structure, with Eae coloured according to the frequency of mutation with respect to the sequence
510 of the crystal structure (P19809). The most frequently mutated residues (observed in > 80
511 isolates) are shown in gold ball-and-stick representation. As discussed above, these mutations
512 consist of one or more mutation types. Of these high frequency mutations, 55% were observed in

513 the D3 domain (Tir binding domain). The variations in the interface residues of Tir (residues 296-
514 315) are shown as blue sticks (Figure 5E).

515 ### 3.3.4 Structural modelling of intimin subtypes

516 In order to investigate the functional consequences of sequence variation, the structures of
517 Intimin-Tir complexes were modelled using AlphaFold3[27]. As noted previously (section 3.2.2)
518 there are ten *eae* genetic subtypes represented in our set of *stx*+/*eae*+ isolates. Therefore, ten
519 structural models were generated corresponding to these *eae* subtypes in complex with their
520 cognate Tir partner. The quality of the modelled complexes is indicated by the ipTM (interface
521 Predicted TM) score, which measures the accuracy of the predicted positions of the subunits in
522 the modelled complex. ipTM scores greater than 0.8 are predictions with high confidence and
523 predictions with ipTM <0.6 are failed predictions[27]. All the modelled complexes except rho and
524 theta have high confidence predictions for the relative subunit positions (Table 3). Therefore for
525 rho and theta subtypes, homology modelling (Modeller v 9.10) was used to generate the Eae-Tir
526 structural complex using PDB structure 1F02 as a template.
527
528 Furthermore, the quality of the Eae-Tir interface of these modelled complexes was assessed
529 using an in-house deep learning based method (DPI-score, Bhujel *et al.*, manuscript under
530 preparation). All the modelled complexes were predicted to have a high quality score for the
531 protein-protein interface (Table 3).
532

533 **Table 3**: Confidence scores for the Eae-Tir modelled complexes. All the complexes except for
534 rho and theta were modelled using AlphaFold3 (AF3). For the subtypes rho and theta, homology
535 modelling was used to model the complex using PDB structure 1F02 as a template. *Interface
536 scores were obtained for AF3 models for all subtypes except rho and theta, for which it is
537 calculated on the homology models generated using Modeller.

Intimin Subtype	ipTM score (AF3 models)	Interface score
gamma	0.88	0.98
alpha	0.83	0.98
beta	0.82	0.96
delta	0.79	0.98
epsilon	0.81	0.98
iota	0.81	0.99
rho	0.34	0.99*
theta	0.17	0.99*
xi	0.83	0.98
zeta	0.83	0.99

538
539
540 Upon validation of the quality of modelled complexes, the effects of genomic variations that were
541 observed at the interface between Intimin and Tir were investigated. The variants present at the
542 interface between Intimin and its cognate Tir were assessed in order to elucidate the gain of
543 interactions required to preserve the receptor binding and maintain function. Some of these co-
544 occurring variations (including two, E312 and N300, of three Eae binding hotspots as listed in
545 Ross and Miller, 2007[56]) and their impacts are highlighted here.

546 E312V(Tir):

547

548 E312(Tir) is a known crucial interface residue (PDB ID: 1F02, Figure 6A) and is identified as one
549 of the intimin binding hotspot residues[56]. In the reference crystal structure, it is observed to interact
550 with K927(Eae) and K298(Tir). In the zeta, alpha and gamma intimin subtypes in our set of non-
551 O157 *eae*+ isolates, their cognate Tir protein sequences were observed to have the mutation
552 E312V (Figures 6B, 6C and 6D respectively). E312V results in the loss of these interactions due
553 to the non-polar side chain of valine.
554

555 However, to counter the effects of this loss of interactions, K927D, K927E and K927N were
556 observed in the zeta, alpha and gamma *eae* subtypes respectively (Figure 6B-D). The
557 neighboring residue, K298(Tir), is a conserved residue and plays a role in preserving the Eae-Tir
558 interactions in the *eae* subtypes. Additionally, S929(Eae) was observed to be mutated to
559 S929N(Eae) in these three subtypes, which help to preserve the interactions with the conserved
560 residue K298. However, out of the three variants, gamma has the least number of compensatory
561 interactions that involve K298 (Figure 6D), although there may be compensatory changes at other
562 interaction sites.

563 N300(Tir)

564 N300(Tir) is another Eae intimin binding hotspot[56] and may form a hydrogen-bond with E930 in
565 the crystal structure (PDB ID: 1F02, Figure 7A). N300(Tir) was observed to be mutated to D, I or
566 S in the isolates having *eae* subtypes zeta, rho and theta respectively. Upon structural inspection,
567 N300D appears to form a salt bridge with E930K in the zeta subtypes (Figure 7B). This pair of
568 co-occurring mutations shows a reversal of residue type, with the glutamic acid of 930(Eae) being
569 replaced by the aspartic acid of 300(Tir), and illustrates the compensation required to maintain
570 function, that is Eae-Tir binding.

571 The structural models for rho and theta produced using AlphaFold 3 predicted a different
572 interaction site between Eae and Tir than the one observed in the crystal structure (1F02, Figures
573 S6A and S6B). To try to obtain the expected quaternary structure, we modelled the complex with
574 AlphaFold 3 including only the D3 region of the Eae subtype sequence together with the Tir
575 extracellular domain. However, superposition of the predicted complex structure with the crystal
576 structure showed many changes in the secondary structure of Eae which are probably artefacts
577 due to the loss of D2 (Figure S6C and S6D). Therefore, it was necessary to resort to the traditional
578 approach of homology modelling using Modeller[41] (v10.4) and the crystal structure as template.

579 These homology models were used to examine the variations in the rho and theta subtypes. There
580 did not appear to be any major impacts of N300S in the theta subtype on the interface between
581 Eae and Tir (Figure 7C), despite the loss of a specific interaction with Eae. E930A is the co-
582 occurring mutation observed in its Eae sequence. For the rho model, no gains of interaction were
583 observed for N300I(Tir). However, the co-occurring mutation E930S(Eae) may form a H-bond
584 with N932 (Eae) to counter the effect of variations and preserve the structure and function (Figure
585 7D).

586 # 4. Discussion

587 In this study, a dataset comprising 286 non-O157 STEC genomes sourced from EnteroBase was
588 curated and analysed to determine whether the virulence factor complement coupled with allelic
589 variation could be used to infer their role in pathogenicity. We used the premise that genetic
590 variation that results in structural changes impacts protein function and potentially their
591 contribution to virulence. A selection of isolates was made to represent a diverse range of
592 serotypes, with highly prevalent and well-characterised serotypes such as O26 excluded to
593 minimise bias. The presence of the *stx* toxin gene was used to define these isolates as STEC.
594 The genomic diversity of the set of non-O157 STEC isolates is illustrated by the fact that the
595 genomes share only 3119 core genes out of a pangenome of ~36k genes.

596 The study took a two-step approach, to first investigate the individual and co-occurrence of
597 genetic factors that are thought to contribute to disease, defined as Virulence Factors[24,25].
598 Secondly, since the majority of virulence factors exist in different allelic variants, the potential
599 functional impact of variation was investigated, focusing on the well characterised STEC virulence
600 factor Intimin, Eae and its cognate partner, Tir. Variations were considered both at the subtype
601 level and at the level of individual point mutations. This serves as an example for other protein
602 interactions of virulence factor variants, and potential impacts on overall pathogenicity of non-
603 O157 STEC isolates.

604 The non-O157 STEC are characterised by their genetic diversity. Using serotype alone as a
605 distinguishing feature identified 111 variants in our dataset. Like other members of the *E. coli*
606 species, it is evident that the STEC sub-species comprise mosaic genomes, with multiple
607 instances of recombination, genomic rearrangements and horizontally acquired elements, making
608 classification challenging. The decision tree from the JEMRA risk matrix is based on the *stx* gene
609 subtype and the presence of the intimin gene, *eae*, and the transcriptional activator of aggregative
610 adherence fimbria expression, *aggR*. However, the intimin gene is not ubiquitous in clinical
611 samples and was only present in 85 / 286 (30 %) *stx*+ non-O157 STEC genomes investigated.
612 Furthermore, *aggR* is not widespread in EHEC and does not occur at all in our *stx*+ set.

613 Some serotypes of STEC that lack initimin are notable as they still cause severe disease[57]. STEC
614 O91 is reported to be one of the most common *eae*- non-O157 serotypes associated with human
615 disease[58]. O91 and O113 have been reported as prevalent serotypes (top 9) in England in 2019[59],
616 and are represented in our dataset. STEC O55 outbreaks have also been reported in England[41],
617 represented by nine *eae*+ isolates and two *eae*- isolates in the dataset .

618 Besides *stx*, and *eae*, additional virulence factors are associated with pathogenicity of non-O157
619 STECs, and can contribute to severe disease phenotypes such as bloody diarrhoea and HUS.
620 Genes that help with adherence, colonisation, production and secretion of toxins are known to be
621 associated with causing severe disease. Within our dataset, there was a large degree of variation
622 in the complement of virulence factors, with 130 different types of virulence factors across the set.
623 Some factors are present in most isolates (e.g. *nlpI, terC, yeh, csgA*), while others are only
624 represented in single isolates, such as *csm* and *fot*. The virulence factors that occurred frequently
625 are known to be abundant in *E. coli* genomes[60]. They can be considered as factors that facilitate
626 host colonisation or adhesion to a surface, and in doing so contribute to pathogenicity and lead
627 to disease.

628 The co-occurrence of some pairs of virulence factors was evident, while other pairs were
629 apparently mutually exclusive in the set of isolates. Several different sets of genes co-occurred,
630 with the largest group encompassing a range of functions associated with virulence, including:
631 *ireA*, a siderophore associated with pathology in UTI[61] ; capsular polysaccharide production
632 genes, *kps*[62]; microcin genes, *mchC* and *F,* associated with virulence in the STEC O91
633 serogroup[63]; the *Shigella* enterotoxin gene *sen,* also associated with bacteraemic *E. coli*
634 isolates[64]; *shiA,* responsible for immunomodulatory functions in *Shigella* species[65], with homologs
635 apparently with similar functions in uropathogenic *E. coli*[66]; the subtilis cytotoxin gene *subA*,
636 associated with STEC[67] including isolates from cattle[68]; and the associated *tia* gene, shown to be
637 involved in cellular invasion of some STEC strains[69]. Notably, the latter two virulence factors are
638 encoded on the subtilase-encoding pathogenicity island (SE-PAI) and are mutually exclusive with
639 the locus for enterocyte effacement[70], presumably because of the role in invasion as opposed to
640 A/E lesion formation.

641 Co-occurrence of virulence factors with the initimin gene, *eae*, was quantified to obtain a clearer
642 indication of potentially interacting networks based on this key virulence factor. 52 % and 41 % of
643 the *eae*+ isolates were *stx2* and *stx1*, respectively, with only 7 % occurring with both *stx*1+ and
644 *stx*2+. As expected, some virulence factors are co-located with intimin on the LEE island e.g. *tir*,
645 *espA, espB, espF*, although not all. This is in-line with the concept of a network of T3SS effectors,
646 which exhibit co-dependency and context-dependent functionality[71]. Virulence factors that
647 exhibited strong co-occurrence with *eae* include the non-LEE encoded T3SS effectors *nleA/B/C*
648 and *cif,* and the plasmid-encoded genes *esp, tox* and *katP*.

649 Several of the genes identified in co-occurrence networks of virulence factors were first identified
650 on the pO157 plasmid, which was genetically characterised in serotype O157:H7, strain Sakai[72].
651 It encodes genes for a type 2 secretion system and the alpha-hemolysin gene cluster, *hyl*[73],as
652 well as its associated protease, *katP*. *katP* has been detected in multiple non-O157 isolates on
653 other plasmids, e.g. in O111[74] and O26[75], with sub-type a in particular associated with clinical
654 disease[76]. It is normally linked with other plasmid encoded virulence factors: the heamolysin gene
655 cluster (*hyl*), a lipid A modification system (*ecf* operon) and the serine protease (*espP*), although
656 they do not always co-occur[74]. The *katP* gene is normally associated with LEE-encoding STEC
657 strains, and not in non-LEE strains, presumably down to genetic incompatibility[77]. The KatP
658 protease is responsible for cleavage and inactivation of Hyl heamolysin. STEC isolates frequently
659 encode multiple hemolysins, of which four have been reported: alpha-hemolysin (HylA),
660 enterohemolysin (ExhA) also encoded on a plasmid or phage (e-HylA) and silent hemolysin /
661 cytolysin A (SheA)[78]. Both HylA and ExhA were detected in the STEC genome dataset.
662 Hemolysins are encoded in other pathotypes of *E. coli*, although there has been shown to be a
663 strong association between both ExhA and HylA and presence of *stx* genes and to some extent,
664 with presence of *eae*[78].

665 Using reference sequences taken from the Virulence Finder database, ten *eae* genetic subtypes
666 were identified across the dataset of 85 isolates. Multiple subtypes of the *eae* gene have been
667 reported previously, and correlated with host specificity and tissue tropism[79]. The *eae* gene was
668 initially sequenced from EPEC lineage 1 strain E2348/69, forming the reference sequence for α-
669 intimin, while EPEC lineage 2 strains encode subtype β-intimin. Further subtypes are defined for
670 EHEC, such as γ-intimin from O157:H7 and O55:H7 strains[80]. Divergent intimins appear to be
671 encoded by mosaic alleles composed of DNA segments with different evolutionary histories[81].

672 Variation in intimin subtypes has long been recognised[81], with at least 18 different genetic variants
673 identified in a single non-O157 STEC genome set[79]. The *eae* variants identified here showed
674 significant identity amongst themselves, with the epsilon and xi subtypes sharing ~97% identity.
675 Recombination events have been implicated in the evolution of *eae*, and split decomposition
676 analysis on this dataset suggested a reticulate network indicative of recombination. The genomic
677 variations (non-synonymous) in intimin subtypes were inspected using the sequence of *eae*-α as
678 reference. ~700 variations were observed in all intimin protein sequences and 78% of these lie in
679 the extracellular region of intimin (domains D1, D2 and D3), which interacts with the receptor Tir.
680 However, the extracellular region of Tir was observed to be more conserved than the extracellular
681 region of intimin.

682 Protein structural modelling enabled a better understanding of the functional implications of the
683 genomic variations. AlphaFold3[27] was used to generate the three-dimensional structural models
684 of the intimin subtypes with their cognate Tir receptor, validated with an in-house machine learning
685 based method. With AlphaFold3, monomeric protein structures are modelled with high accuracy
686 although protein-protein complexes modelling is still a developing analytical tool[82]. As such, three-
687 dimensional structure modelled complexes need to be validated using confidence metrics such
688 as pLDDT (per atom confidence score), ipTM (confidence in relative placement of subunits in a
689 modelled complex). Although the structures are models and the atom positions are approximate,
690 it nonetheless still provides a good estimate of interactions at the interface.

691 Mapping of Eae variations onto structural models shows that most occur in the extra-cellular
692 domains, and of these most are in the interaction region with the cognate partner Tir. Mutations
693 in the extra-cellular region may be associated with immune escape, but nevertheless binding with
694 Tir must be maintained in order to retain effective pedestal formation. For some specific examples,
695 we have shown that variations preserve the functional interaction between the two protein
696 partners through a compensatory mechanism, wherein loss of some interactions at the interface
697 is compensated by the formation of new interfacial contacts. Understanding the importance of
698 specific interactions involved in receptor binding will help improve the interpretation of STEC
699 genomic variants and may aid the development of interventions.

700 Through this work, we would like to emphasise the importance of integrating genomic analysis
701 with protein structural analysis which provides insights into mechanism of function, in this case
702 pathogenicity of eae+ STEC isolates. The examples of co-occurring variations at protein-protein
703 interfaces underscore the importance of integrating genomic data with structural biology to
704 deepen our understanding of protein function.

705

Funding

This work was supported by STFC Food Safety Network+ (award R24686 to NH and MW), Food Safety Research Network (award 43266FSRN-2023S12 to NH), and AIBIO-UK ((22-AIBN) [BB/Y006933/1]) Pilot funding, round1 (to SM).

Author Contributions

Sony Malhotra- Conceptualization, Formal analysis, Funding acquisition, Methodology, Writing-original draft, Writing- review and editing
Ashley Ward- Data curation
Lauren Giles- Data curation, Writing- review and editing
Tom Gerrard- Formal Analysis
Martyn Winn- Conceptualization, Formal analysis, Funding acquisition, Methodology, Writing-original draft, Writing- review and editing
Nicola Holden- Conceptualization, Data curation, Funding acquisition, Methodology, Project Administration, Writing-original draft, Writing- review and editing

Conflict of Interest

None

References

1. Shiga toxin-producing Escherichia coli (STEC) data: 2024 - GOV.UK. https://www.gov.uk/government/publications/escherichia-coli-e-coli-o157-annual-totals/shiga-toxin-producing-escherichia-coli-stec-data-2024.
2. Shiga toxin-producing Escherichia coli (STEC) data: 2023. *GOV.UK* https://www.gov.uk/government/publications/escherichia-coli-e-coli-o157-annual-totals/shiga-toxin-producing-escherichia-coli-stec-data-2023.
3. King, G. *et al.* Epidemiology of Shiga toxin-producing Escherichia coli other than serotype O157:H7 in England, 2016–2023. *Journal of Medical Microbiology* **74**, 001947 (2025).
4. Panel, E. B. *et al.* Pathogenicity assessment of Shiga toxin-producing Escherichia coli (STEC) and the public health risk posed by contamination of food with STEC. *EFSA Journal* **18**, e05967 (2020).
5. Shiga toxin-producing Escherichia coli (STEC) and food: attribution, characterization, and monitoring: report. https://www.who.int/publications/i/item/9789241514279.
6. FAO/WHO STEC EXPERT GROUP. Hazard Identification and Characterization: Criteria for Categorizing Shiga Toxin-Producing Escherichia coli on a Risk Basis†. *J Food Prot* **82**, 7–21 (2019).
7. Rauw, K. D., Buyl, R., Jacquinet, S. & Piérard, D. Risk determinants for the development of typical haemolytic uremic syndrome in Belgium and proposition of a new virulence typing algorithm for Shiga toxin-producing Escherichia coli. *Epidemiology & Infection* **147**, e6 (2019).
8. Fuller, C. A., Pellino, C. A., Flagler, M. J., Strasser, J. E. & Weiss, A. A. Shiga Toxin Subtypes Display Dramatic Differences in Potency. *Infection and Immunity* **79**, 1329–1337 (2011).
9. Gallegos, K. M. *et al.* Shiga Toxin Binding to Glycolipids and Glycans. *PLoS One* **7**, e30368 (2012).

752 10. Goffaux, F., China, B., Janssen, L., Pirson, V. & Mainil, J. The locus for enterocyte
753 effacement (LEE) of enteropathogenic Escherichia coli (EPEC) from dogs and cats. *Adv Exp*
754 *Med Biol* **473**, 129–136 (1999).
755 11. IRSHAD, H., COOKSON, A. L., PRATTLEY, D. J., DUFOUR, M. & FRENCH, N. P.
756 Distribution of Escherichia coli strains harbouring Shiga toxin-producing E. coli (STEC)-
757 associated virulence factors (stx1, stx2, eae, ehxA) from very young calves in the North
758 Island of New Zealand. *Epidemiol Infect* **142**, 2548–2558 (2014).
759 12. Rodwell, E. V. *et al.* Epidemiology and genomic analysis of Shiga toxin-producing
760 Escherichia coli clonal complex 165 in the UK. *J Med Microbiol* **70**, 001471 (2021).
761 13. Slater, S. L., Sågfors, A. M., Pollard, D. J., Ruano-Gallego, D. & Frankel, G. The Type III
762 Secretion System of Pathogenic Escherichia coli. *Curr Top Microbiol Immunol* **416**, 51–72
763 (2018).
764 14. Gauthier, A., de Grado, M. & Finlay, B. B. Mechanical fractionation reveals structural
765 requirements for enteropathogenic Escherichia coli Tir insertion into host membranes. *Infect*
766 *Immun* **68**, 4344–4348 (2000).
767 15. Battle, S. E., Brady, M. J., Vanaja, S. K., Leong, J. M. & Hecht, G. A. Actin Pedestal
768 Formation by Enterohemorrhagic Escherichia coli Enhances Bacterial Host Cell Attachment
769 and Concomitant Type III Translocation. *Infection and Immunity* **82**, 3713–3722 (2014).
770 16. Croxen, M. A. & Finlay, B. B. Molecular mechanisms of Escherichia coli pathogenicity.
771 *Nat Rev Microbiol* **8**, 26–38 (2010).
772 17. Paganini, J. A. *et al.* Predicting clinical outcome of Escherichia coli O157:H7 infections
773 using explainable Machine Learning. 2025.06.05.25329036 Preprint at
774 https://doi.org/10.1101/2025.06.05.25329036 (2025).
775 18. Shiga toxin-producing Escherichia coli (STEC) data: 2022. *GOV.UK*
776 https://www.gov.uk/government/publications/escherichia-coli-e-coli-o157-annual-totals/shiga-
777 toxin-producing-escherichia-coli-stec-data-2022.

19. Gastrointestinal and Zoonoses - Biennial report 2020 to 2021 - Gastrointestinal and Zoonoses - Publications - Public Health Scotland. https://publichealthscotland.scot/publications/gastrointestinal-and-zoonoses/gastrointestinal-and-zoonoses-biennial-report-2020-to-2021/.

20. Data and surveillance - Shiga toxin-producing Escherichia coli (STEC) - Infectious diseases - Health protection - Population health - Public Health Scotland. https://publichealthscotland.scot/population-health/health-protection/infectious-diseases/shiga-toxin-producing-escherichia-coli-stec/data-and-surveillance/.

21. Dyer, N. P. *et al.* EnteroBase in 2025: exploring the genomic epidemiology of bacterial pathogens. *Nucleic Acids Research* **53**, D757–D762 (2025).

22. Ishii, S., Meyer, K. P. & Sadowsky, M. J. Relationship between Phylogenetic Groups, Genotypic Clusters, and Virulence Gene Profiles of Escherichia coli Strains from Diverse Human and Animal Sources. *Applied and Environmental Microbiology* **73**, 5703–5710 (2007).

23. Bhattacharyya, A., Panday, S. & Ussery, D. Rapid assessment of clinical severity for salmonellosis cases via protein family domain analysis and machine learning. *Academia Molecular Biology and Genomics* **2**, (2025).

24. Malberg Tetzschner, A. M., Johnson, J. R., Johnston, B. D., Lund, O. & Scheutz, F. In Silico Genotyping of Escherichia coli Isolates for Extraintestinal Virulence Genes by Use of Whole-Genome Sequencing Data. *Journal of Clinical Microbiology* **58**, 10.1128/jcm.01269-20 (2020).

25. Joensen, K. G. *et al.* Real-Time Whole-Genome Sequencing for Routine Typing, Surveillance, and Outbreak Detection of Verotoxigenic Escherichia coli. *Journal of Clinical Microbiology* **52**, 1501–1510 (2014).

26. Roe, A. J., Hoey, D. E. E. & Gally, D. L. Regulation, secretion and activity of type III-secreted proteins of enterohaemorrhagic Escherichia coli O157. *Biochemical Society Transactions* **31**, 98–103 (2003).

804 27. Abramson, J. *et al.* Accurate structure prediction of biomolecular interactions with
805 AlphaFold 3. *Nature* **630**, 493–500 (2024).
806 28. Leinonen, R., Sugawara, H. & Shumway, M. The Sequence Read Archive. *Nucleic Acids*
807 *Res* **39**, D19–D21 (2011).
808 29. BBMap. *SourceForge* https://sourceforge.net/projects/bbmap/ (2025).
809 30. Langmead, B. & Salzberg, S. L. Fast gapped-read alignment with Bowtie 2. *Nat Methods*
810 **9**, 357–359 (2012).
811 31. Li, H. *et al.* The Sequence Alignment/Map format and SAMtools. *Bioinformatics* **25**,
812 2078–2079 (2009).
813 32. Prjibelski, A., Antipov, D., Meleshko, D., Lapidus, A. & Korobeynikov, A. Using SPAdes
814 De Novo Assembler. *Curr Protoc Bioinformatics* **70**, e102 (2020).
815 33. Seemann, T. Prokka: rapid prokaryotic genome annotation. *Bioinformatics* **30**, 2068–
816 2069 (2014).
817 34. Camacho, C. *et al.* BLAST+: architecture and applications. *BMC Bioinformatics* **10**, 421
818 (2009).
819 35. Gertz, E. M., Yu, Y.-K., Agarwala, R., Schäffer, A. A. & Altschul, S. F. Composition-
820 based statistics and translated nucleotide searches: Improving the TBLASTN module of
821 BLAST. *BMC Biology* **4**, 41 (2006).
822 36. Edgar, R. C. MUSCLE: a multiple sequence alignment method with reduced time and
823 space complexity. *BMC Bioinformatics* **5**, 113 (2004).
824 37. Stamatakis, A. RAxML version 8: a tool for phylogenetic analysis and post-analysis of
825 large phylogenies. *Bioinformatics* **30**, 1312–1313 (2014).
826 38. Tonkin-Hill, G. *et al.* Producing polished prokaryotic pangenomes with the Panaroo
827 pipeline. *Genome Biology* **21**, 180 (2020).
828 39. Moore, R. M., Harrison, A. O., McAllister, S. M., Polson, S. W. & Wommack, K. E. Iroki:
829 automatic customization and visualization of phylogenetic trees. *PeerJ* **8**, e8584 (2020).

830 40. Huson, D. H. & Bryant, D. The SplitsTree App: interactive analysis and visualization
831 using phylogenetic trees and networks. *Nat Methods* **21**, 1773–1774 (2024).
832 41. Sali, A. Comparative protein modeling by satisfaction of spatial restraints. *Mol Med*
833 *Today* **1**, 270–277 (1995).
834 42. Panel, E. B. *et al.* Pathogenicity assessment of Shiga toxin-producing Escherichia coli
835 (STEC) and the public health risk posed by contamination of food with STEC. *EFSA Journal*
836 **18**, e05967 (2020).
837 43. Bugarel, M., Beutin, L. & Fach, P. Low-Density Macroarray Targeting Non-Locus of
838 Enterocyte Effacement Effectors (nle Genes) and Major Virulence Factors of Shiga Toxin-
839 Producing Escherichia coli (STEC): a New Approach for Molecular Risk Assessment of
840 STEC Isolates. *Appl Environ Microbiol* **76**, 203–211 (2010).
841 44. Coombes, B. K. *et al.* Molecular Analysis as an Aid To Assess the Public Health Risk of
842 Non-O157 Shiga Toxin-Producing Escherichia coli Strains. *Appl Environ Microbiol* **74**, 2153–
843 2160 (2008).
844 45. Loukiadis, E. *et al.* Distribution, functional expression, and genetic organization of Cif, a
845 phage-encoded type III-secreted effector from enteropathogenic and enterohemorrhagic
846 Escherichia coli. *J Bacteriol* **190**, 275–285 (2008).
847 46. Tsutsuki, H. *et al.* Subtilase cytotoxin from Shiga-toxigenic *Escherichia coli* impairs the
848 inflammasome and exacerbates enteropathogenic bacterial infection. *iScience* **25**, 104050
849 (2022).
850 47. Navarro-Garcia, F. *et al.* Pic, an Autotransporter Protein Secreted by Different
851 Pathogens in the Enterobacteriaceae Family, Is a Potent Mucus Secretagogue. *Infect Immun*
852 **78**, 4101–4109 (2010).
853 48. Christenson, J. K. & Gordon, D. M. Evolution of colicin BM plasmids: the loss of the
854 colicin B activity gene. *Microbiology* **155**, 1645–1655 (2009).
855 49. Boerlin, P. *et al.* Associations between virulence factors of Shiga toxin-producing

856 Escherichia coli and disease in humans. *J Clin Microbiol* **37**, 497–503 (1999).
857 50. Werber, D. *et al.* Strong association between shiga toxin-producing Escherichia coli
858 O157 and virulence genes stx2 and eae as possible explanation for predominance of
859 serogroup O157 in patients with haemolytic uraemic syndrome. *Eur J Clin Microbiol Infect Dis*
860 **22**, 726–730 (2003).
861 51. Melton-Celsa, A. R., Kokai-Kun, J. F. & O'Brien, A. D. Activation of Shiga toxin type 2d
862 (Stx2d) by elastase involves cleavage of the C-terminal two amino acids of the A2 peptide in
863 the context of the appropriate B pentamer. *Molecular Microbiology* **43**, 207–215 (2002).
864 52. Croxen, M. A. & Finlay, B. B. Molecular mechanisms of Escherichia coli pathogenicity.
865 *Nat Rev Microbiol* **8**, 26–38 (2010).
866 53. Creuzburg, K. *et al.* Evolutionary analysis and distribution of type III effector genes in
867 pathogenic Escherichia coli from human, animal and food sources. *Environ Microbiol* **13**,
868 439–452 (2011).
869 54. Luo, Y. *et al.* Crystal structure of enteropathogenic Escherichia coli intimin-receptor
870 complex. *Nature* **405**, 1073–1077 (2000).
871 55. Vieira, M. F. M. *et al.* The pathogen-encoded signalling receptor Tir exploits host-like
872 intrinsic disorder for infection. *Commun Biol* **7**, 1–21 (2024).
873 56. Ross, N. T. & Miller, B. L. Characterization of the binding surface of the translocated
874 intimin receptor, an essential protein for EPEC and EHEC cell adhesion. *Protein Sci* **16**,
875 2677–2683 (2007).
876 57. Feng, P., Delannoy, S., Lacher, D. W., Bosilevac, J. M. & Fach, P. Characterization and
877 Virulence Potential of Serogroup O113 Shiga Toxin–Producing *Escherichia coli* Strains
878 Isolated from Beef and Cattle in the United States. *Journal of Food Protection* **80**, 383–391
879 (2017).
880 58. Bielaszewska, M. *et al.* Shiga Toxin, Cytolethal Distending Toxin, and Hemolysin
881 Repertoires in Clinical Escherichia coli O91 Isolates. *Journal of Clinical Microbiology* **47**,

882 2061 (2009).
883 59. Shiga toxin-producing Escherichia coli (STEC) data: 2019. *GOV.UK*
884 https://www.gov.uk/government/publications/escherichia-coli-e-coli-o157-annual-totals/shiga-
885 toxin-producing-escherichia-coli-stec-data-2019.
886 60. Touchon, M. *et al.* Organised Genome Dynamics in the Escherichia coli Species Results
887 in Highly Diverse Adaptive Paths. *PLOS Genetics* **5**, e1000344 (2009).
888 61. Hagan, E. C. & Mobley, H. L. T. Uropathogenic Escherichia coli Outer Membrane
889 Antigens Expressed during Urinary Tract Infection. *Infection and Immunity* **75**, 3941–3949
890 (2007).
891 62. Russo, T. A., Wenderoth, S., Carlino, U. B., Merrick, J. M. & Lesse, A. J. Identification,
892 Genomic Organization, and Analysis of the Group III Capsular Polysaccharide Genes kpsD,
893 kpsM,kpsT, and kpsE from an Extraintestinal Isolate of Escherichia coli (CP9, O4/K54/H5).
894 *Journal of Bacteriology* **180**, 338–349 (1998).
895 63. Nüesch-Inderbinen, M. *et al.* Distribution of virulence factors, antimicrobial resistance
896 genes and phylogenetic relatedness among Shiga toxin-producing Escherichia coli serogroup
897 O91 from human infections. *Int J Med Microbiol* **311**, 151541 (2021).
898 64. Telli, M. *et al.* Prevalence of enterotoxins among Escherichia coli isolates causing
899 bacteraemia. *FEMS Microbiol Lett* **306**, 117–121 (2010).
900 65. Ingersoll, M. A. *et al.* The ShiA protein encoded by the Shigella flexneri SHI-2
901 pathogenicity island attenuates inflammation. *Cellular Microbiology* **5**, 797–807 (2003).
902 66. Lloyd, A. L., Smith, S. N., Eaton, K. A. & Mobley, H. L. T. Uropathogenic Escherichia coli
903 Suppresses the Host Inflammatory Response via Pathogenicity Island Genes sisA and sisB.
904 *Infection and Immunity* **77**, 5322–5333 (2009).
905 67. Paton, A. W., Srimanote, P., Talbot, U. M., Wang, H. & Paton, J. C. A New Family of
906 Potent AB5 Cytotoxins Produced by Shiga Toxigenic Escherichia coli. *J Exp Med* **200**, 35–46
907 (2004).

908 68. Cáceres, M. E., Etcheverría, A. I., Fernández, D., Rodríguez, E. M. & Padola, N. L.
909 Variation in the Distribution of Putative Virulence and Colonization Factors in Shiga Toxin-
910 Producing Escherichia coli Isolated from Different Categories of Cattle. *Front. Cell. Infect.*
911 *Microbiol.* **7**, (2017).
912 69. Bondì, R. *et al.* The Gene tia, Harbored by the Subtilase-Encoding Pathogenicity Island,
913 Is Involved in the Ability of Locus of Enterocyte Effacement-Negative Shiga Toxin-Producing
914 Escherichia coli Strains To Invade Monolayers of Epithelial Cells. *Infection and Immunity* **85**,
915 10.1128/iai.00613-17 (2017).
916 70. Michelacci, V. *et al.* A new pathogenicity island carrying an allelic variant of the Subtilase
917 cytotoxin is common among Shiga toxin producing Escherichia coli of human and ovine
918 origin. *Clinical Microbiology and Infection* **19**, E149–E156 (2013).
919 71. Sanchez-Garrido, J., Ruano-Gallego, D., Choudhary, J. S. & Frankel, G. The type III
920 secretion system effector network hypothesis. *Trends Microbiol* **30**, 524–533 (2022).
921 72. Makino, K. *et al.* Complete Nucleotide Sequences of 93-kb and 3.3-kb Plasmids of an
922 Enterohemorrhagic Escherichia coli O157:H7 Derived from Sakai Outbreak. *DNA Res* **5**, 1–9
923 (1998).
924 73. Brockmeyer, J. *et al.* Enterohaemorrhagic Escherichia coli haemolysin is cleaved and
925 inactivated by serine protease EspPα. *Environmental Microbiology* **13**, 1327–1341 (2011).
926 74. Ogura, Y. *et al.* Comparative genomics reveal the mechanism of the parallel evolution of
927 O157 and non-O157 enterohemorrhagic Escherichia coli. *Proceedings of the National*
928 *Academy of Sciences* **106**, 17939–17944 (2009).
929 75. Fratamico, P. M. *et al.* The complete DNA sequence and analysis of the virulence
930 plasmid and of five additional plasmids carried by Shiga toxin-producing *Escherichia coli*
931 O26:H11 strain H30. *International Journal of Medical Microbiology* **301**, 192–203 (2011).
932 76. Khan, A. B. *et al.* Serine protease *espP* subtype *α*, but not *β* or *γ*, of Shiga toxin-
933 producing *Escherichia coli* is associated with highly pathogenic serogroups. *International*

934 *Journal of Medical Microbiology* **299**, 247–254 (2009).
935 77. Newton, H. J. *et al.* Shiga Toxin–producing Escherichia coli Strains Negative for Locus
936 of Enterocyte Effacement. *Emerg Infect Dis* **15**, 372–380 (2009).
937 78. Lorenz, S. C. *et al.* Prevalence of Hemolysin Genes and Comparison of ehxA Subtype
938 Patterns in Shiga Toxin-Producing Escherichia coli (STEC) and Non-STEC Strains from
939 Clinical, Food, and Animal Sources. *Applied and Environmental Microbiology* **79**, 6301–6311
940 (2013).
941 79. Yang, X. *et al.* Genetic diversity of the intimin gene (eae) in non-O157 Shiga toxin-
942 producing Escherichia coli strains in China. *Sci Rep* **10**, 3275 (2020).
943 80. Fitzhenry, R. J. *et al.* Tissue Tropism of Enteropathogenic Escherichia coli Strains
944 Belonging to the O55 Serogroup. *Infection and Immunity* **70**, 4362–4368 (2002).
945 81. McGraw, E. A., Li, J., Selander, R. K. & Whittam, T. S. Molecular evolution and mosaic
946 structure of alpha, beta, and gamma intimins of pathogenic Escherichia coli. *Mol Biol Evol* **16**,
947 12–22 (1999).
948 82. Lu, D., Yu, S., Huang, Y. & Gong, X. Multimeric protein interaction and complex
949 prediction: Structure, dynamics and function. *Comput Struct Biotechnol J* **27**, 1975–1997
950 (2025).
951
952

953 ## Figure Legends

954

955 **Figure 1**: Collection of non-O157 STEC isolates (n=286) and virulence factor mapping. **A**.
956 Distribution of different serotypes in the collection of non-O157 STEC genomes from the clinical
957 isolates obtained from the Enterobase. **B**. Presence of different types of *stx* in these serotypes.
958 **C**. Histogram of number of virulence factors in non-O157 STEC genomes. **D**. Subtypes of *stx*
959 toxin genes in non-O157 STEC genomes.

960

961 **Figure 2**: Virulence factors presence and co-occurence in the set of isolates. **A.** Most frequent
962 virulence factors (present in at least 50% of the genomes). **B.** Co-occurrence of virulence
963 factors in our set of 281 isolates. The diagonal gives the absolute number of isolates that a
964 virulence factor occurs in. The off-diagonal entries give the number of isolates containing both
965 virulence factors (corresponding to the row and the column), given as a fraction of the total
966 number of isolates that the virulence factor on the row occurs in. Note that this definition means
967 that the matrix is asymmetric.

968

969 **Figure 3**: Co-occurrence of *stx* and *eae* genes. **A**. Distribution of intimin subtypes in *stx*
970 subtypes. **B**. Distribution of *stx* subtypes in intimin negatives isolates.

971

972 **Figure 4**: Phylogenetic tree for **A**. Core genome of 286 non-O157 STEC isolates, **B**. 85 *eae*+ LEE
973 sequences. The LEE sequence from STEC O157 Sakai is labeled as 'LEE' in the phylogeny. **C.**
974 Secretin C protein from the LEE of 85 *eae*+ isolates. Secretin C protein from the STEC O157
975 Sakai is labeled as 'LEE' in the phylogeny, and **D**. 31 unique *eae* sequences from *eae* +isolates
976 (n=85). The leaf labels are colored according to the *eae* subtypes (eae negative:black,
977 alpha:brown, beta:limegreen, gamma:orange, delta:magenta, rho:pink, iota:orange, delta:violet,
978 epsilon:red, iota:wheat, theta:yellow, xi:cyan, zeta:royalblue), the bar length depicts the number
979 of virulence factors present in the genome and the leaf node color is colored according to the
980 Shiga Toxin subtype (*stx1*: grey, *stx2*: teal, *stx1* and *stx2*: brown).

981

982 **Figure 5:** Variations in the intimin amino acid sequences. **A**. Schematic of Eae domains, domain
983 boundaries are marked. **B**. Number of variations in different intimin domains. **C**. Number and
984 types of variations of interface residues present in Eae's D3. The number of Eae sequences with
985 mutation is shown as orange bar and the height of blue bar denotes the types of variations
986 observed for that particular interface residue. **D.** 15 types of variations in the beta hairpin region

of Tir, which is known to interact with Eae. **E.** Structural mapping of variations observed in Eae (salmon) and the Eae-binding region of Tir (green). The variations in Eae are colored according to their frequency; 1< frequency <=20 (brown), 21< frequency <=40 (gray), 41< frequency <=60 (teal), 61< frequency <=80 (yellow) and frequency >80 (golden sticks).

Figure 6: Structural inspection of interactions between Eae-Tir (Tir:E312 and Eae: K927 and K 928). **A**. As in the crystal structure, 1F02, the residue E312(tir) sits at the interface with Eae and interacts with K298 and K927. **B**. In the zeta subtype, E312V results in the loss of these interactions but simultaneously the gain of interactions is observed due to the other variations in *eae* namely K927D and S929N to preserve the interactions at the interface. **C.** In the alpha subtype,the co-occurring variations K927E and S929N in Eae were observed to gain interactions at the interface. **D**. In the gamma subtype, E312V, there were no notable gain in interactions.

Figure 7: Structural inspection of interactions between Eae-Tir (Tir: N300 and Eae: E930). **A**. N300 is seen to be in proximity to E930 and they may be involved in H-bond. **B.** In zeta subtype, this interaction is seen to be preserved by the formation of salt bridge between the residues N300D and E930K. **C**. In theta subtype, N300S and E930A are observed however no specific gain of interaction is observed upon the mutation. **D**. In the rho subtype, N300I is observed along with E930S. E930S may be forming a H-bond with N932 to maintain the structural stability of the Eae.

Supplementary Material

Figure S1: Co-occurrence of selected gene groups. Gene group '*aal*' includes 4 genes, '*fae*' includes 6 genes, and '*mch*' includes 2 genes, giving a total of 32 genes.

Figure S2: Pairwise percent identity between the protein sequences of 10 intimin subtypes plotted as a heatmap.

Figure S3: **A**. The phylogeny obtained using the aligned core genome sequences of the LEE obtained from the *eae*+ isolates (n = 85). Split decomposition network tree using **B**. full length intimin sequences, **C**. N-terminus region (1-700) and **D**. C-terminus region (701-939) of the intimin sequences.

Figure S4: Split decomposition network tree using **A**. N-terminus region (1-550) and **B**. C-terminus region of the intimin sequences.

Figure S5: Full length structural model of Intimin. **A**. Full length structural model for the UniProt sequence P19809 (Intimin) obtained using AlphaFold3. The sequence domains are colored: sp(yellow), LysM(orange), β-barrel(magenta), D0 and D00(blue), D1 (orange red), D2(cyan) and D3 (red). The point mutation sites are shown as black sticks. **B**. PAE (predicted aligned error) plot of the structural model obtained using AlphaFold3.

Figure S6: Different structure prediction approaches for Eae-Tir sequences. The crystal structure (PDB ID: 1F02) in all the panels is shown in green (Tir) and salmon (Eae). **A**. Structural model of the translated rho Eae-Tir (blue) complex modelled using AlphaFold3 is superposed over the crystal structure. The interface modelled for the rho subtype is different to the one observed in crystal structure. **B**. Structural model of only D3 region of rho subtype with its cognate Tir built using AlphaFold3. The modelled complex is in blue. **C.** The structural model of the theta Eae-Tir (yellow) complex modelled using AlphaFold3 is superposed over the crystal structure. The interface modelled for the theta subtype is different to the one observed in crystal structure. **D**. Structural model of only D3 region (yellow) of theta subtype with its cognate Tir built using AlphaFold3.

1041 **Table S1**: Distribution of non-O157 STEC serotypes in the human isolates in the UK obtained
1042 from Enterobase.
1043
1044 **Table S2**: Accession IDs (Enterobase) of the non-O157 STEC isolates used in the study.
1045
1046 **Table S3:** Virulence factor genes (using 3 letter nomenclature) in non-O157 STEC isolate
1047 genomes (n=286). Their presence in intimin positive isolates, enrichment factor and Jaccard
1048 similarity is also listed.
1049
1050 **Table S4**: Virulence factor genes (using 4 letter nomenclature) in non-O157 STEC isolate
1051 genomes (n=286). Their presence in intimin positive isolates, enrichment factor and Jaccard
1052 similarity is also listed.

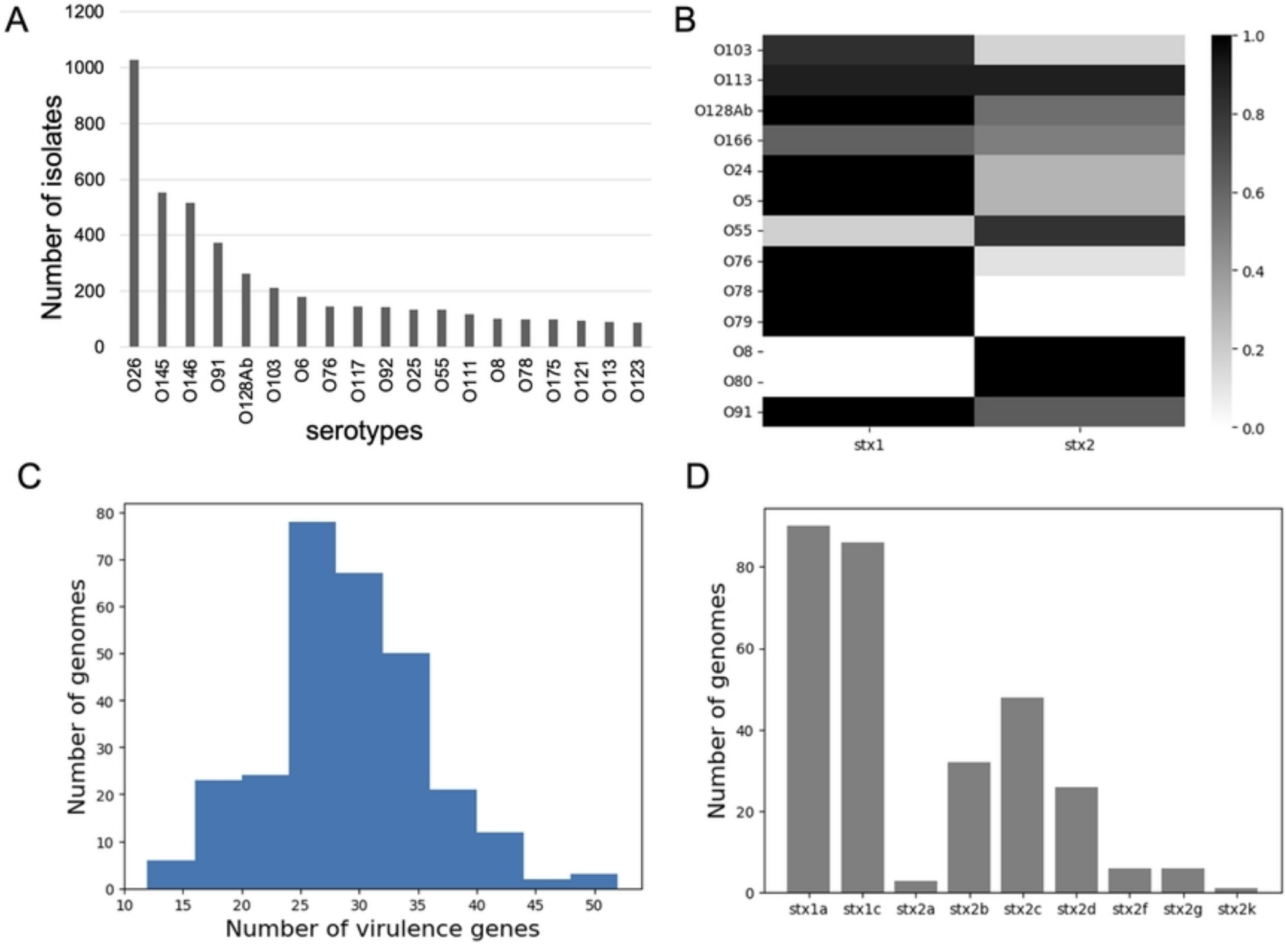
A
Number of isolates
1200
1000
800
600
400
200
0
O26
O145
O146
O91
O128Ab
O103
O6
O76
O117
O92
O25
O55
O111
O8
O78
O175
O121
O113
O123
serotypes
B
O103
O113
O128Ab
O166
O24
O5
O55
O76
O78
O79
O8
O80
O91
stx1
stx2
1.0
0.8
0.6
0.4
0.2
0.0
C
Number of genomes
80
70
60
50
40
30
20
10
0
10
15
20
25
30
35
40
45
50
Number of virulence genes
D
Number of genomes
80
60
40
20
0
stx1a
stx1c
stx2a
stx2b
stx2c
stx2d
stx2f
stx2g
stx2k

Figure 1

A.

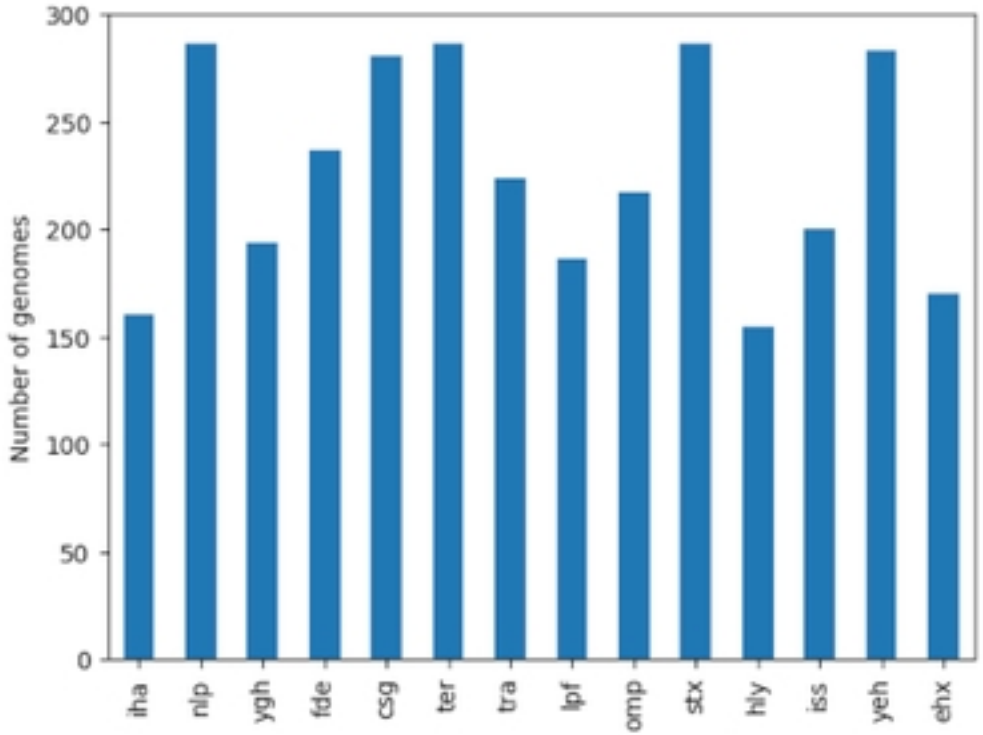
Number of genomes
300
250
200
150
100
50
0
iha
nlp
ygh
fde
csg
ter
tra
lpf
omp
stx
hly
iss
yeh
ehx

B.

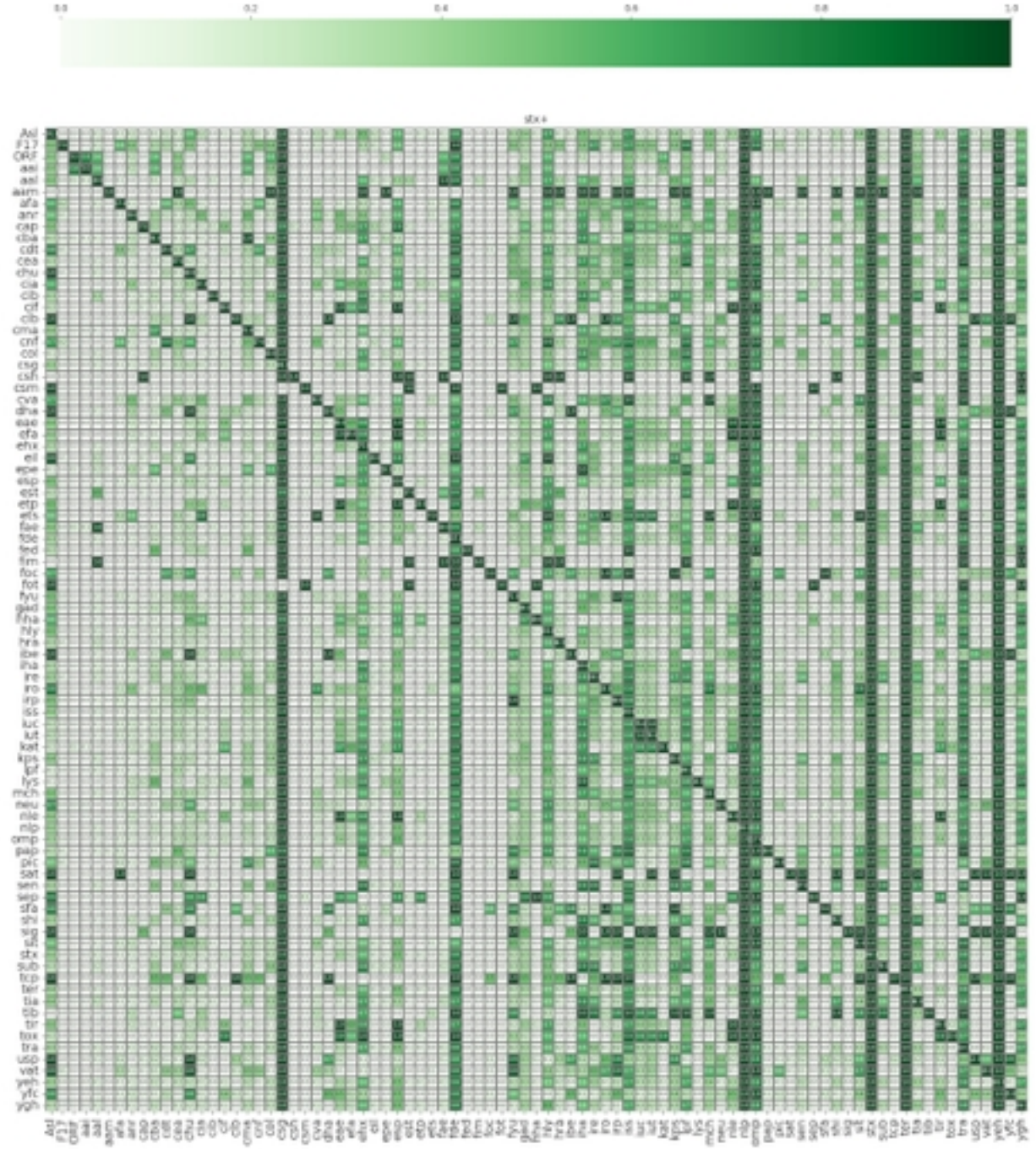

Figure 2

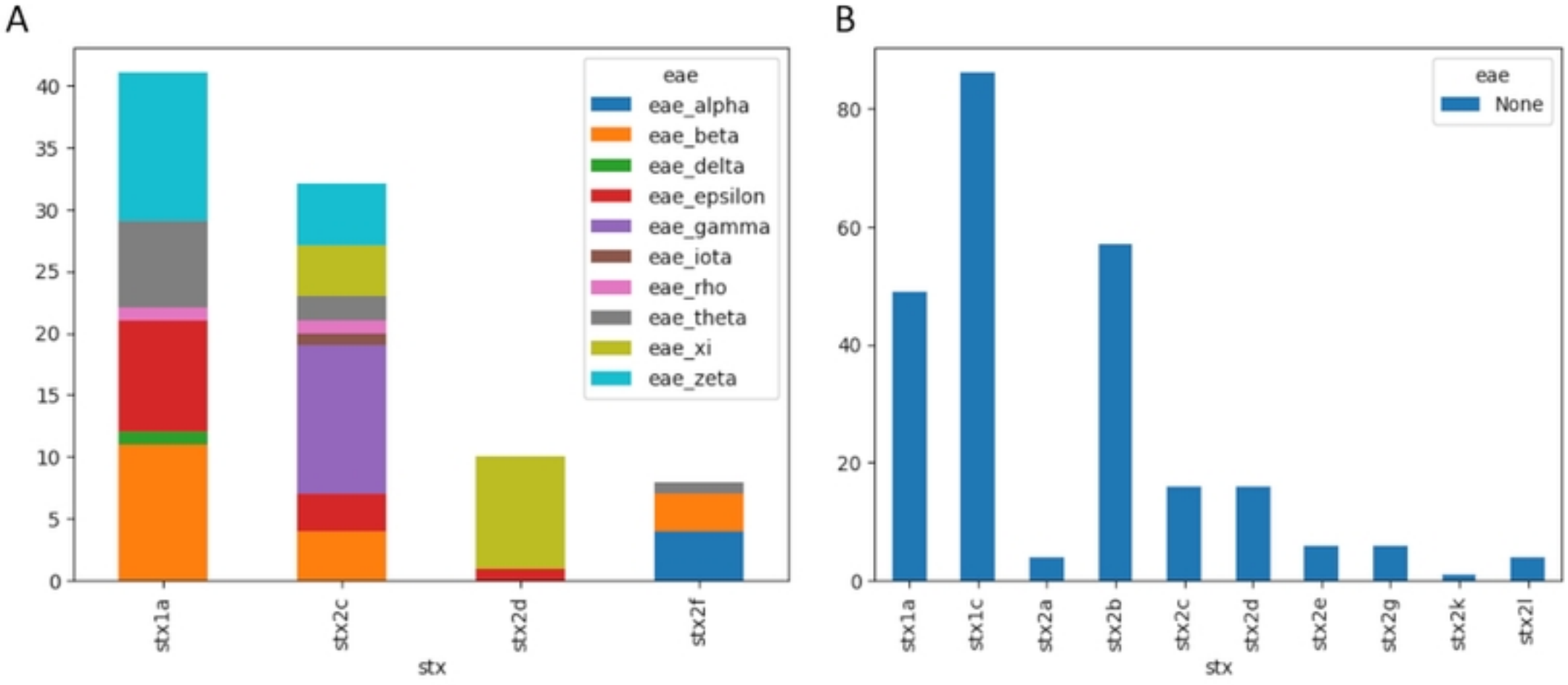
A
B
eae
eae_alpha
eae_beta
eae_delta
eae_epsilon
eae_gamma
eae_iota
eae_rho
eae_theta
eae_xi
eae_zeta
0
5
10
15
20
25
30
35
40
stx1a
stx2c
stx2d
stx2f
stx
eae
None
0
20
40
60
80
stx1a
stx1c
stx2a
stx2b
stx2c
stx2d
stx2e
stx2g
stx2k
stx2l
stx

Figure 3

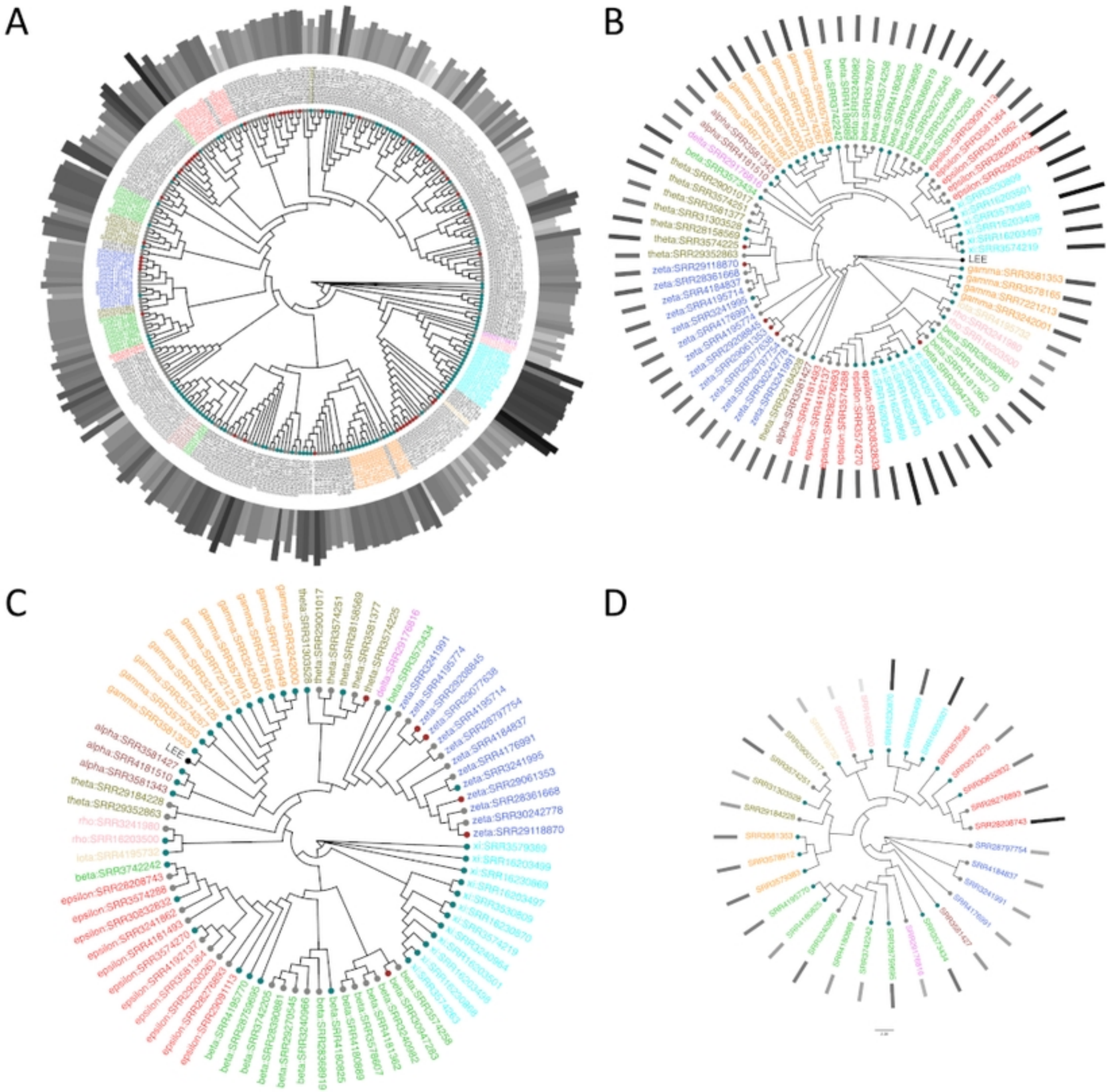

Figure 4

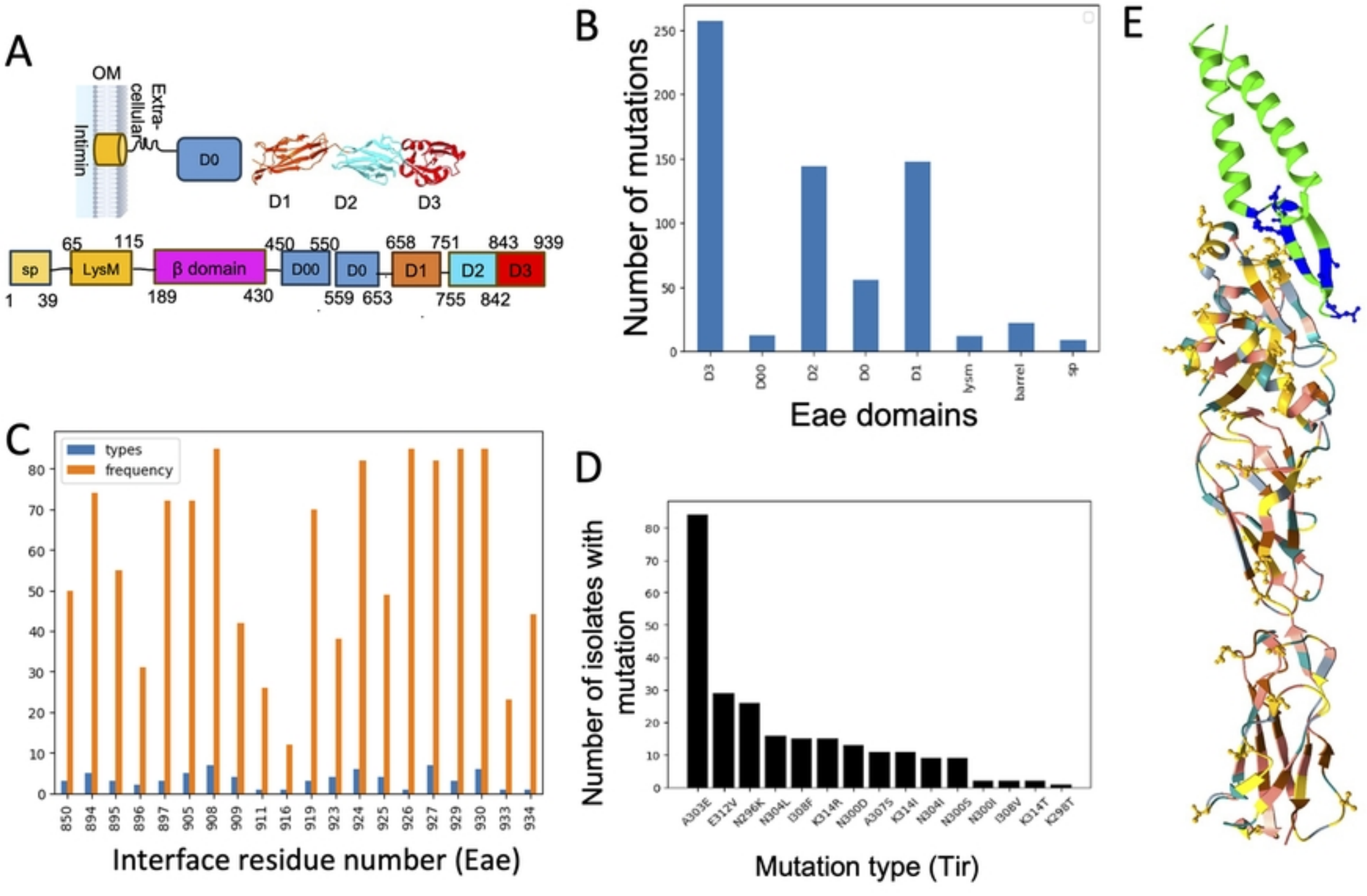
A
OM
Extra-cellular
Intimin
D0
D1
D2
D3
sp
LysM
β domain
D00
D0
D1
D2
D3
1
39
65
115
189
430
450
550
559
653
658
751
755
842
843
939
B
Number of mutations
Eae domains
D3
D00
D2
D0
D1
lysm
barrel
sp
C
types
frequency
Interface residue number (Eae)
850
894
895
896
897
905
908
909
911
916
919
923
924
925
926
927
929
930
933
934
D
Number of isolates with mutation
Mutation type (Tir)
A303E
E312V
N296K
N304L
I308F
K314R
N300D
A307S
K314I
N304I
N300S
N300I
I308V
K314T
K298T
E

Figure 5

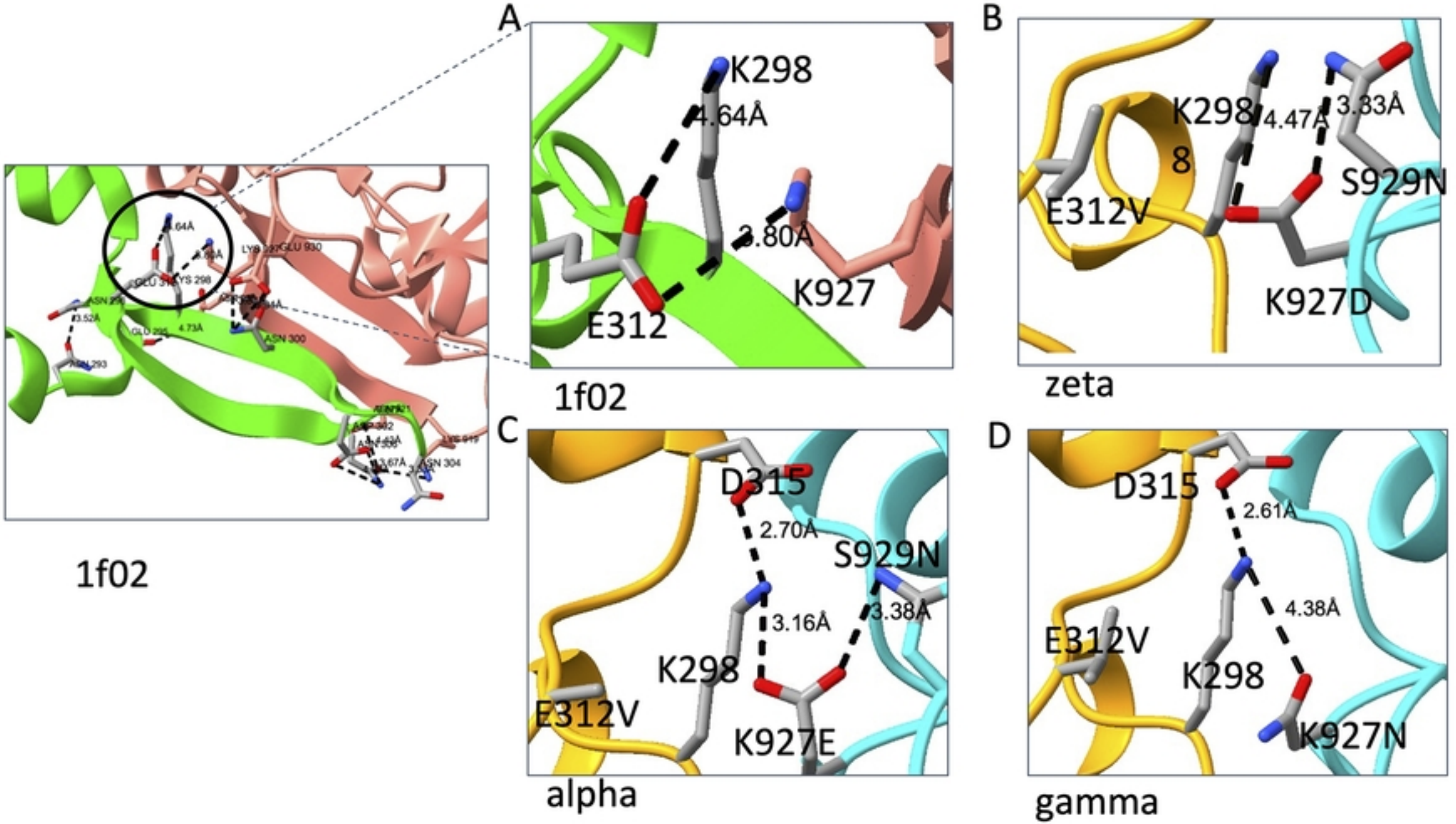
A
K298
4.64Å
3.80Å
K927
E312
1f02
B
K298
8
4.47Å
3.33Å
S929N
E312V
K927D
zeta
C
D315
2.70Å
S929N
3.16Å
3.38Å
K298
E312V
K927E
alpha
D
D315
2.61Å
4.38Å
E312V
K298
K927N
gamma
1f02

Figure 6

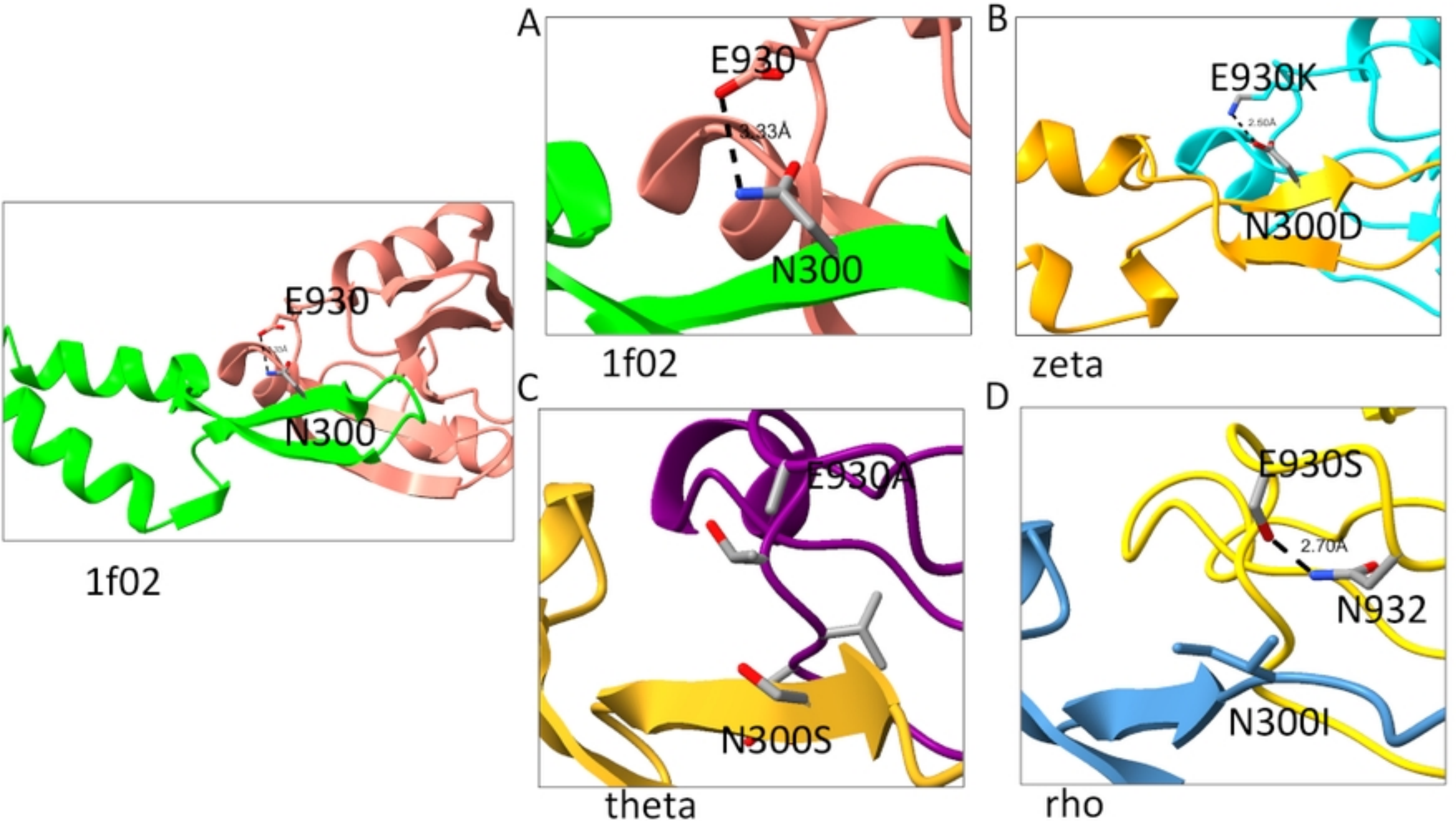
E930
N300
1f02
A
E930
3.33Å
N300
1f02
B
E930K
2.60Å
N300D
zeta
C
E930A
N300S
theta
D
E930S
2.70Å
N932
N300I
rho

Figure 7